

# Flexural fatigue behaviour of recycled tyre polymer fibre reinforced concrete

Meng Chen<sup>a</sup>, Hui Zhong<sup>b</sup>, Mingzhong Zhang<sup>b,\*</sup>

<sup>a</sup> *School of Resource and Civil Engineering, Northeastern University, Shenyang, 110819, China*

<sup>b</sup> *Department of Civil, Environmental and Geomatic Engineering, University College London, London, WC1E 6BT, UK*

**Abstract:** The utilization of recycled tyre polymer fibre (RTPF) into concrete production is feasible to promote sustainable development and mitigate environmental pollution of global landfilled waste tyres. This paper for the first time presents an experimental study on flexural fatigue behaviour of concrete reinforced with mixed RTPF considering different fibre dosages (i.e., 1.2, 2.4, 4.8 and 9.6 kg/m<sup>3</sup>). Results indicate that with the presence of RTPF, the flexural strength of concrete was increased by 3.6-9.6%. The fatigue life of all mixtures followed the two-parameter Weibull distribution and can be accurately predicted using the developed double-logarithm fatigue equations. Concrete reinforced with 4.8 kg/m<sup>3</sup> of RTPF presented the longest fatigue life under different failure probabilities. RTPF and polypropylene fibre (PPF) reinforced concrete exhibited similar fatigue failure mechanisms. 0.2-0.4%  $V_f$  of RTPF could substitute around 0.1%  $V_f$  of PPF in concrete considering overall static, dynamic and fatigue performance.

Keywords: Fibre reinforced concrete; Recycled fibre; Polypropylene fibre; S-N curve; Microstructure

## 1. Introduction

Fibre reinforced concrete (FRC) is a composite material mainly exhibiting superior crack-resistant and post-cracking performance [1-3]. In practice, FRC is commonly employed in pavements (e.g. airport and highway), bridge decks, tunnel linings and offshore platform [4-6], which may suffer from repetitive cyclic loading during its entire service life. Thus, the fatigue behaviour of FRC is critically essential as it may fail due to the combination of its internal formed cracks induced by shrinkage or creep and increasingly developed cracks caused by the fatigue loading [7]. In addition, the mechanical performance and durability of FRC subjected to cyclic loading may degrade gradually until reaching its ultimate failure point [4], in which the service life of the structures made of such FRC would be accordingly reduced leading to increasing maintenance cost.

In the past several decades, numerous studies have explored the fatigue behaviour of FRC wherein

---

\* Corresponding author. E-mail address: mingzhong.zhang@ucl.ac.uk (M. Zhang)

various types of fibres were incorporated including steel [8-13], polypropylene [14-17], polyvinyl alcohol [5, 18, 19] and carbon [20, 21] fibres, which generally suggested that the incorporation of the above fibres with a suitable dosage improved the fatigue performance of concrete considering different conditions, e.g., stress ratio, stress level and specified material properties. Given the fact that the results of fatigue test are normally discrete [10, 22] and therefore, two-parameter Weibull distribution is widely employed to statistically analyse the fatigue life of FRC [5, 8, 10, 11, 23-26]. Li et al. [5] investigated the compressive fatigue behaviour of ultra-high toughness cementitious composite (UHTCC) and found that the fatigue life of UHTCC followed the two-parameter Weibull distribution. Singh and Kaushik [8] studied the fatigue behaviour of concrete reinforced with 1.5% fibre volume fraction ( $V_f$ ) of steel fibre and concluded that the equivalent fatigue life of steel-FRC was in consistence with the two-parameter Weibull distribution. The high correlation between fatigue life and two-parameter Weibull distribution for FRC was also observed in [10, 11, 13, 23-26]. Moreover, the parameters of Weibull distribution were applied to predict the fatigue life of concrete under a particular stress level with different failure probabilities. For instance, Goel and Singh [10] adopted the parameters of Weibull distribution to predict the fatigue life of self-compacting concrete reinforced with steel fibre considering different failure probabilities and noted that, the presence of steel fibres enhanced the overall fatigue behaviour of concrete. Singh and Kaushik [8], Wang et al. [13] and Lv et al. [26] developed double-logarithm fatigue equations based on the parameters of Weibull distribution to predict the flexural fatigue strength of FRC for a specific survival probability. In addition, probabilistic analyses were performed to better understand the fatigue behaviour of FRC. For instance, Castillo and Canteli [27] demonstrated a unified methodology to derive models for fatigue life considering three main fatigue approaches including stress-based, strain-based and fracture mechanics approaches. Saucedo et al. [28] developed a probabilistic fatigue model capable of handling various loading frequencies and stress ratios for plain concrete and FRC, which was further validated by Ríos et al. [29] based on the experimental flexural fatigue results for both plain concrete and FRC. It can be concluded that the fatigue equation and model are essential for the characterization and analysis of fatigue behaviour of FRC, which can in turn provide a solid foundation for the structural design considering its fatigue performance.

Nevertheless, the increasing energy consumption (about 15% of the total building energy) and generated environmental pollution by manufacturing the aforementioned fibres [30-32] motivated

researchers to explore the possibility of utilizing end-of-life materials (e.g. waste tyres) as fibre reinforcement constituents. In particular, recycled tyre polymer fibre (RTPF) extracted from end-of-life tyres through thermomechanical processes is regarded as a promising recycled material [33], which can be incorporated into concrete for the sake of improving FRC's sustainability and mitigating the environmental impact caused by landfilling the waste tyres (approximately 500 million landfilled waste tyres every year [34]). Recently, a few studies [35-41] have been carried out to estimate the effect of RTPF on mechanical properties (static and dynamic) and durability performance of normal concrete. Baričević et al. [35, 36] concluded that the incorporation of RTPF can reduce the early-age shrinkage deformation of concrete and enhance its resistance to freeze-thaw cycles. Serdar et al. [37], and Onuaguluchi and Banthia [39] also observed the improvement in shrinkage resistance (plastic and autogenous) for mixture reinforced with RTPF. Huang et al. [38] found the significant enhancement in fire resistance for RTPF-FRC. Chen et al. [40] recently explored the effect of varying RTPF dosages on dynamic compressive behaviour of concrete and concluded that the addition of RTPF led to an obvious improvement (about 6.6%-12.9%) in dynamic compressive strength and energy absorption capacity at various strain rates and the optimal mixed RTPF dosage was recommended as  $2.4 \text{ kg/m}^3$  (i.e. 0.2%  $V_f$ ). Onuaguluchi and Banthia [41] concluded that RTPF combining with either hooked-end steel or polypropylene fibre (PPF) can create positive synergy in post-crack flexural performance, which could be used as a sprayed repair material for certain structures (e.g. bridge decks and tunnels). Besides, it was found that the manufactured PPF could be replaced by RTPF considering dynamic compressive behaviour. The mechanical properties and durability performance of RTPF-FRC have been increasingly studied but up to now, no extensive investigation has been done on fatigue performance of concrete reinforced with RTPF. Thus, a comprehensive study of fatigue behaviour of RTPF-FRC is urgently needed.

This paper aims to investigate the flexural fatigue behaviour of RTPF-FRC considering two main influencing factors, i.e. stress level and fibre content. Firstly, fresh and hardened properties of all mixtures including workability, air content, compressive strength and flexural strength were measured and the effect of RTPF content on these properties was evaluated. Secondly, flexural fatigue tests were conducted using four various stress levels (i.e., 0.90, 0.85, 0.80 and 0.75) and the corresponding fatigue life data of each mixture was processed using the two-parameter Weibull distribution. The average Weibull distribution parameters were derived accordingly based on three different approaches

to predict the fatigue life of all mixtures corresponding to various failure probabilities, and the fatigue equations were then developed. Lastly, the fatigue damage process and failure mode of all mixtures under different stress levels were discussed with the help of scanning electron microscopy (SEM) images for the morphology of the fibres. An in-depth comparison between RTPF- and PPF-FRC regarding static and flexural fatigue performance was also demonstrated.

## 2. Experimental program

### 2.1 Raw materials

Portland cement (P.I. 42.5) was used as binder material for all tested mixtures in this study, the specific gravity of which is 3.09. The chemical compositions of cement are listed in [Table 1](#). Natural river sand with a specific gravity of 2.56 was used as fine aggregate. The particle size distributions of cement and sand are shown in [Fig. 1](#). Crushed granites with a maximum size of 20 mm were used as coarse aggregate. Polycarboxylate-based superplasticisers (SPs) were used whilst mixing to ensure sufficient consistency for all mixtures.

[Fig. 2](#) shows the single-filament PPF and RTPF (i.e. as-received RTPF with rubber granules attached) used in this work. The RTPF provided by Jinghan rubber and plastic products Co. Ltd in Shanghai was recycled mainly from truck tyres and its main compositions are 52% polyethylene terephthalate (PET), 39% polyamide 66 (PA 66) and 9% polybutylene terephthalate (PBT) [40]. It should be noted that several rubber granules attached the RTPF and thus, a simplified method based on the previous study by Baričević et al. [35] was applied to estimate the composition of RTPF. [Fig. 3](#) shows a schematic diagram of the process of estimating the composition of RTPF. Firstly, three sieves with different openings (i.e. 0.315, 0.63 and 1.25 mm) were placed on a vibration table. RTPFs were placed in the sieve with an opening of 1.25 mm and six steel balls with a diameter of 8 mm were applied to improve the efficiency of separating the cleaned RTPFs (i.e. RTPFs with only tiny amount of rubber granules attached) from the rubber granules. Due to the gravitational forces, very fine cleaned RTPFs and rubber particles fell into the 0.63 mm or 0.315 mm sieves. Later, an airscrew was adopted to separate the cleaned RTPFs from some big rubber particles in the 1.25 mm sieve. The above procedure was repeated six times. The weight ratio of cleaned RTPF and rubber granules shown in [Fig. 3](#) was found to be 56.8% and 43.2%, respectively [40]. [Fig. 2c](#) and [d](#) show the SEM images of PPF and RTPF indicating that PPF is straighter than RTPF, while the dimension of RTPFs is not uniform. Hence, microscopic investigation was conducted to determine the length distribution of

RTPF. 500 samples were selected for characterizing the length of RTPF, the length distribution of which is illustrated in **Fig. 4**. The diameter of RTPF was measured using a fibre diameter tester (XGD-1 Fibre Diameter Tester). 300 samples were tested, and the average value was accordingly obtained. The mechanical properties (e.g. tensile strength) of RTPF were measured using a fibre tensile tester (XQ-1A Fibre Tensile Tester) in accordance with GB/T 21120-2007 [42]. Herein, 50 samples of RTPF were tested and an average value was determined. Differential scanning calorimetry (DSC) measurement was carried out to estimate the melting point of RTPF. The properties of PPF and RTPF are listed in **Table 2** [40].

## 2.2 Mix design and specimen preparation

As explained in a previous study [40], four different RTPF dosages ranging from  $1.2 \text{ kg/m}^3$  (0.1%  $V_f$ ) to  $9.6 \text{ kg/m}^3$  (0.8%  $V_f$ ) were adopted in this study to determine the optimal RTPF content in terms of flexural fatigue performance. A control mixture (no fibre incorporation) was prepared and denoted as F0. Previous studies [35-37, 40] illustrated that normal concrete reinforced with an appropriate amount of RTPF presented better performance than that reinforced with PPF considering dynamic compressive properties and early-age shrinkage resistance. Nevertheless, no literature is found regarding the comparison of flexural fatigue behaviour between RTPF-FRC and PPF-FRC. Thus,  $0.9 \text{ kg/m}^3$  (0.1%  $V_f$ ) of PPF was incorporated into concrete to explore whether PPF can be replaced by RTPF in FRC in terms of fatigue behaviour. All mixture proportions investigated in this study are presented in **Table 3**.

With respect to mixing process, all solid ingredients except fibres were firstly mixed for 2 min. Then, water and SPs were gradually added into the mixture. To avoid fibre balling and ensure a good fibre distribution, PPFs or RTPFs were only added until the mixture reached a consistent state. In the case of RTPF-FRC, RTPFs were first mixed with part of water and SPs and then slowly added into the wet mix [39]. After this, fresh mixtures were poured into specific moulds and then placed in a vibration table. For each mixture shown in **Table 3**, 3 cubes with size of 150 mm (for compressive strength test), 3 prisms with size of  $100 \times 100 \times 400 \text{ mm}$  (for flexural strength test) and 20 prisms with size of  $100 \times 100 \times 400 \text{ mm}$  (for flexural fatigue test) were cast. All specimens were demoulded after 24 h of casting and then placed in a standard curing room ( $20 \pm 2 \text{ }^\circ\text{C}$  and 95% RH). The detailed testing program showing the number of conducted tests for each mixture is illustrated in **Table 4**.

## 2.3 Test methods

### 2.3.1 Workability and air content

The workability of all mixtures was determined by conducting the slump test in accordance with GB/T50080-2016 [43]. During the test, fresh concrete mixtures were poured into the testing mould at three layers and jolted for 25 times at each layer. The measurement of slump should start 30 s after the testing mould was filled. The slump value was interpreted as the vertical difference in displacement between the top surface of fresh mixtures and the top of the testing mould.

The air content of all fresh mixtures was measured following ASTM C231-17a [44] using a Type-B meter. Firstly, the aggregate correction factor was determined independently. The air content of each fresh mixture was then calculated using Eq. (1).

$$A_s = A_1 - G \quad (1)$$

where  $A_s$  is the air content of each fresh mixture (%),  $A_1$  is the air content shown by the Type-B meter, and  $G$  is aggregate correction factor (%).

### 2.3.2 Compressive strength

Following GB/T50081-2002 [45], the 28-d compressive strength was tested on three 150 mm cubic specimens by a universal testing machine with a constant loading rate of 9 kN/s. The result of the specimen should be discarded if it is 15% larger or smaller than the median result.

### 2.3.3 Flexural performance under static and fatigue loadings

Before conducting the fatigue tests, it is important to accurately determine the flexural strength of all mixtures. Hence, according to GB/T50081-2002 [45], the static flexural strength of each mixture was measured by an EHF-UV closed loop electrohydraulic universal testing machine shown in [Fig. 5](#). The flexural strength of each mixture can be calculated using Eq. (2).

$$f_f = \frac{FL}{bd^2} \quad (2)$$

where  $f_f$  is the flexural strength of each specimen (MPa),  $F$  is the ultimate load indicated by the testing machine (kN),  $L$  is the test span of the specimen (300 mm),  $b$  is the width of the specimen (100 mm), and  $d$  is the depth of the specimen (100 mm).

Four different stress levels ( $S$ ) including 0.90, 0.85, 0.80 and 0.75 were considered, where  $S$  stands for the ratio of maximum fatigue stress to mean flexural strength. The stress ratio,  $R = f_{min}/f_{max}$ , was kept constant as 0.10 for all fatigue tests conducted in this study, where  $f_{min}$  and  $f_{max}$  represent the minimum and maximum stress applied in the cycle respectively corresponding to the minimum

and maximum force (i.e.  $F_{min}$  and  $F_{max}$ ), as illustrated in **Fig. 6**. All fatigue tests were performed under load control with a constant frequency of 5 Hz in sinusoidal waveform. In addition, strain gauges were attached to the base of the tested specimen (see **Fig. 5**) to measure the change of deformation (i.e. at the upper stress level) throughout the entire fatigue testing. For each mixture, five samples were prepared for each stress level to ensure the reliability of the results. A previous study by Ortega et al. [46] stated that the observed error in experimental fatigue life is related to the number of fatigue tests performed and the desired safety level, i.e., the higher the number of performed tests, the lower the potential error would exist in the result. This study aims to evaluate the effect of RTPF on the trend of fatigue behaviour as a pioneer, in order to further explore the feasibility of applying RTPF in cementitious materials. Thus, the potential error caused by the number of performed tests was not considered in this work.

#### 2.3.4 Microstructure investigation

After the fatigue test, several fracture pieces were chosen from the failure plane of the specimen for SEM test (Ultra-plus SEM, Germany) to explore the surface condition and bridging of RTPF or PPF within the matrix after fatigue failure.

### 3. Results and discussion

#### 3.1 Workability and air content

**Fig. 7** shows the workability of all mixtures. It can be observed that the slump value declined from 185 mm (F0) to 70 mm (RTPF96) implying that the presence of mixed RTPF affected the workability of fresh concrete mixture immediately after the mixing. This can be ascribed to the increasing shear resistance due to the addition of fibres and higher viscosity on account of the lower water-to-binder (w/b) ratio [40]. Whilst mixing, some water may be used to moist the RTPF, which is temporarily blocked inside the RTPF [37]. Moreover, the rubber particles inside the RTPFs have relatively rougher surface (i.e. some pores may exist on the surface) after the tyre recycling treatment [47] and thus, a tiny amount of water may store inside the rubber particles through the pores, particularly for particles with finer size [40]. The combined action can lead to the loss of mixing water, and thereby affecting the slump value of FRC. Besides, the slump value of PPF09 was found to be lower than that of RTPF12 (around 7.6%), which suggests that the detrimental effect of PPF on the workability of normal concrete was more serious than that of RTPF when the fibre volume fraction was equal.

The air content of all mixtures is illustrated in **Fig. 8**. Considering the effect of RTPF, the air

content of fresh concrete mixture was increased with the increase of RTPF dosage. It should be noted that the air content of F0 was around 1.88%, while the air content of RTPF12, RTPF24, RTPF48 and RTPF96 was increased by 11.2%, 17.6%, 27.1% and 47.9%, respectively, as compared with the reference mixture. A similar finding was reported in the previous study [35], which can be ascribed to the extra air entrained by the rubber particles attached the RTPFs during the mixing process [36, 48, 49]. Moreover, the addition of fibres whilst mixing may also entrap some air [50]. As shown in **Fig. 8**, PPF induced higher air content to the fresh concrete as the air content of PPF09 was approximately 15.3% higher than that of RTPF12 (i.e. under the same fibre volume fraction, 0.1%  $V_f$ ), which could be attributed to the larger surface area of PPF in comparison with RTPF (see **Table 2**).

### 3.2 Compressive and flexural strengths

**Fig. 8** shows the 28-d compressive strength of all mixtures. A conspicuous trend can be found that the compressive strength of concrete declined with increasing RTPF content, where the highest addition of RTPF (i.e. 9.6 kg/m<sup>3</sup>) significantly weakened the compressive strength of normal concrete (approximately 17.7%) at 28 d. This phenomenon can be primarily attributed to the reduced workability resulting in a non-uniform distribution of fibres inside the mixture [40]. In addition to this, as mentioned in Section 3.1, the increased air content in RTPF-FRC mainly caused by the incorporation of RTPF and attached rubber particles contributed to the reduction in compressive strength (especially for the particles with a larger size [51]). A clear trend was observed in **Fig. 8** that the compressive strength of RTPF-FRC was reduced with the increase of air content in fresh sample. Furthermore, the porosity and microcrack density are accordingly enhanced due to the incorporation of fibres, which leads to a lower strength property [4]. To make a comparison with previous studies, a summary regarding the influence of RTPF or crumb rubber on compressive strength is shown in **Fig. 9**. The results here are in consistence with the previous research [35] that the compressive strength of concrete reduced with the presence of RTPF. Besides, the increasing amount of crumb rubber inside the mixture contributes to the reduction of compressive strength [47, 52-55] (see **Fig. 9**) primarily due to its lower stiffness and density. PPF generated more negative effect on the compressive strength than RTPF under the equal fibre volume fraction (about 3.6% lower than that of RTPF12), which proves the feasibility of using RTPF to replace PPF in FRC.

The 28-d flexural strength of all mixtures is presented in **Fig. 10**. Generally, the incorporation of

RTPF improved the flexural strength of concrete regardless of fibre content. As compared with F0 (plain reference mixture), the flexural strength of RTPF12, RTPF24, RTPF48 and RTPF96 increased by 3.6%, 9.6%, 7.3% and 5.6%, respectively. The improvement in flexural strength can be attributed to the enhanced resistance to crack development across the fracture zone, which shows good agreement with Baričević et al. [35, 36] that the inclusion of RTPF can help reduce the early-age shrinkage deformation of concrete, and thereby increasing its tensile capacity and accordingly decreasing its crack width caused by the shrinkage mechanism. It is worth noting that fibre bridging action at the cracking zone plays an important role in improving the flexural strength of concrete, especially when more fibres are perpendicular to the fracture surface [56, 57], which implies that the flexural strength is significantly influenced by the fibre content and fibre orientation in the concrete mixture. Besides, it can be seen from Fig. 10 that RTPF24 reached the highest flexural strength, while continuous incorporation of RTPF (i.e. 4.8 and 9.6 kg/m<sup>3</sup>) slightly weakened the positive influence generated by the RTPF (around 2.1% and 3.6% lower than that of RTPF24). However, the difference between RTPF24 and RTPF48 was not significant (approximately 0.11 MPa). The flexural strength reduction observed in RTPF96 may be owing to the reduced workability (decreased by 62.2% compared to F0), which results in lower compactness and higher porosity of mixture caused by the non-uniform distribution of the fibres. The poor distribution of fibres may influence the bonding between the fibre and the matrix, and therefore reducing the efficiency of fibre bridging action and subsequently affecting the corresponding flexural strength [58, 59]. Considering the same fibre volume fraction (0.1%  $V_f$ ), the 28-d flexural strength of RTPF12 was 4.8% smaller than that of PPF09, which showed good agreement with [29] that longer fibres are more effective in improving the flexural strength under a certain fibre volume fraction (i.e. 1.0-1.5%  $V_f$ ). This may suggest that RTPF with shorter length has poorer crack-bridging capability since the fibre with a longer length tends to bridge a crack with a larger size [60] and also, it could improve the interfacial bonding with the matrix [9, 61]. However, RTPF24 (0.2%  $V_f$ ) presented slightly larger flexural strength than PPF09 (0.1%  $V_f$ ). Although the difference is not significant, it still supports the conclusion drawn by Chen et al. [40] that PPF can be replaced by a higher quantity of RTPF if solely considering specific concrete properties.

### 3.3 Flexural fatigue behaviour

#### 3.3.1 Probability distribution

**Fig. 11** shows the probability distribution of all mixtures at different stress levels. The fatigue life ( $N$ ) represents the number of cycles to failure during the flexural fatigue testing and  $P_f$  denotes the empirical failure probability, which can be calculated as follows:

$$P_f = \frac{i}{K+1} \quad (3)$$

where  $i$  is the failure order number and  $K$  stands for the sample size at a given stress level ( $S$ ).

It can be observed from **Fig. 11** that the fatigue results are discrete for each specified stress level. By evaluating the influence of stress level, a similar trend can be identified for all mixtures that the fatigue life increased with decreasing stress level, where previous research [9, 10, 14, 15, 22, 29] observed similar phenomenon for FRC. This can be ascribed to the increasing rate for the formation of initiated microcracks and higher crack propagation rate induced by cyclic loading with a larger stress level and thereby, more cumulative cracks are presented inside the concrete, which finally speeds up the ultimate failure of the concrete. Generally, fatigue damage process can be spilt into three stages [62]: (1) initiation of the microcracks along with the volume deformation of the specimen; (2) steady crack propagation subjected to cyclic loading; (3) simultaneous formation of microcracks and macrocracks prior to final failure of concrete. With the presence of fibres, the formation and development of microcracks can be restricted through the fibre bridging action resulting in a longer fatigue life. Moreover, the crumb rubber attached the RTPF may act as an energy absorber during the fatigue loading if an effective bond arises between rubber particles and concrete matrix [63]. Consequently, a proportion of energy is absorbed by the rubber granules leading to higher amount of energy required to completely fracture the concrete specimen.

#### 3.3.2 Weibull distribution analysis

Previous studies [8, 10, 23-26] found that the flexural fatigue life of FRC followed the two-parameter Weibull distribution. Hence, in this study, the two-parameter Weibull distribution was used to analyse the fatigue life of all mixtures. Firstly, it is critical to determine whether the fatigue life of each mixture at all stress levels follows the two-parameter Weibull distribution.

The functions of survival probability ( $P$ ) and failure probability ( $P_f$ ) corresponding to a particular value of fatigue life ( $N$ ) for Weibull distribution can be expressed as follows [64, 65]:

$$P = e^{-\left(\frac{N}{N_a}\right)^a} \quad (4)$$

$$P_f = 1 - e^{-\left(\frac{N}{N_a}\right)^a} \quad (5)$$

where  $N_a$  represents the characteristic life or scale parameter and  $a$  is the shape parameter of the Weibull distribution.

The empirical survival probability ( $P$ ) can be expressed by [8]:

$$P = 1 - \frac{i}{K+1} \quad (6)$$

By taking the logarithm twice of both sides of Eq. (4), the following equation can be obtained.

$$\ln \left[ \ln \left( \frac{1}{P} \right) \right] = a \ln N - a \ln N_a \quad (7)$$

Eq. (7) can be considered as a linear function of  $Y = aX - c$  where  $Y = \ln(\ln(\frac{1}{P}))$ ,  $X = \ln N$  and  $c = a \ln N_a$ , respectively, which was used to determine whether the fatigue life of each mixture follows the two-parameter Weibull distribution under different stress levels [8]. Hence, the curves of the function for all mixtures are shown in **Fig. 12**, along with the corresponding correlation coefficients ( $r$ ) listed in **Table 5**. It can be found clearly that the values of all  $r$  are close to 1 (ranging from 0.9131 to 0.9935) suggesting very reliable correlation for the curves illustrated in **Fig. 12**. Based on this criterion, it verifies that the fatigue performance of all mixtures follows the two-parameter Weibull distribution. To predict the fatigue life ( $N_p$ ) of each mixture, it is necessary to estimate the characteristic life ( $N_a$ ) and shape parameter ( $a$ ), which are the two important input parameters for predicting the fatigue life. **Table 5** demonstrates the results of characteristic life and shape parameter of all mixtures under various stress levels obtained using the graphical method (see **Fig. 12**). Except the graphical method, two other approaches (i.e. method of maximum likelihood estimate and method of moments [8]) were adopted to calculate the corresponding characteristic life and shape parameter. In terms of maximum likelihood estimate, the detailed calculation process can be found in [23, 66]. Regarding the method of moments, the shape parameter ( $a$ ) and characteristic life ( $N_a$ ) can be determined using the following equations [8, 23, 66-68]:

$$a = \beta^{-1.08} \quad (8)$$

$$N_a = \frac{\mu}{T\left(\frac{1}{a}+1\right)} \quad (9)$$

where  $\beta$  represents the coefficient of variation of the data sample under consideration (i.e. ratio of standard deviation and mean),  $\mu$  denotes the sample mean of the data at a given stress level ( $S$ ), and

$T()$  is the gamma function.

A summary of the results of shape parameter and characteristic life derived by three different methods is listed in **Table 5**. **Fig. 13** presents the effect of stress level on the shape parameter of Weibull distribution where no clear trend can be found for each mixture. It is worth mentioning that the shape parameter reflects the discrete level of fatigue life data [29], which means the higher the shape parameter, the lower the discrete level. As observed, the shape parameters of all mixtures were generally lower when the stress ratio was 0.75, ranging from 0.5698 to 0.7094. In particular, F0 had the lowest value at that stress ratio, which may be due to its inhomogeneous nature (i.e. pores and internal cracks are existed randomly). Moreover, more voids existed in the bottom of the prism could lead to smaller cycles to failure [69], which may be also a factor of high discrete level of fatigue data. Although the inhomogeneity of FRC is also high as compared with the mixture without fibre reinforcement, the fibre bridging action across the cracking zone improves the fatigue behaviour of concrete. As a consequence, the ultimate cycles to failure tend to be closer between each specimen. However, the shape parameter of RTPF96 was the lowest (i.e. 0.6489) among all FRC, which could be due to the increased voids around the fibres [29]. No clear trend can be found in terms of the effect of fibre content on the shape parameter when the stress level was 0.80 and 0.85, respectively. By contrast, at the highest stress level (i.e. 0.90 in this study), the shape parameters were generally higher (in the range between 0.8160 and 1.1159), which reveals that the fatigue life data of concrete is less discrete when the stress level is higher [66].

### 3.3.3 Prediction of fatigue life

For engineering practice, it is essential to predict the fatigue life of applied material under different failure probabilities and develop corresponding fatigue equations for estimating its flexural fatigue strength. Accordingly, the predicted fatigue life ( $N_p$ ) was obtained using the following equation [24, 67]:

$$N_p = N_a \left| \ln(1 - P_f) \right|^{\frac{1}{a}} \quad (10)$$

**Fig. 14** presents the S- $N_p$  relationship of all mixtures. As observed, all mixtures exhibited a similar trend that the predicted fatigue life decreased with increasing stress level under different failure probabilities, which is in consistence with the results shown in **Fig. 11**. The predicted fatigue life of each FRC mixture (except RTPF12) was higher than that of plain reference mixture under various

failure probabilities. Considering various failure probabilities and stress levels, the most life increments (in terms of logarithm form) of RTPPF12, RTPPF24, RTPPF48, RTPPF96, PPF09 ranged from 3.3-25.1%, 32.5-49.9%, 22.9-58.3%, 6.6-37.5% and 13.5-50.0%, respectively as compared with F0, where the inclusion of 2.4 kg/m<sup>3</sup> and 4.8 kg/m<sup>3</sup> of RTPPF induced better performance in enhancing the fatigue life. The results here are consistent with previous research [5, 10, 26] that the addition of fibres enhanced the fatigue life of concrete or mortar considering different stress levels or varying reliabilities, which can be explained by the bridging action of fibre across the cracking zone. Under a good fibre orientation, the efficiency of fibre bridging action tends to be higher with the presence of internal microcracks. As stated before, the initiation of increasing quantity of microcracks mostly happens in the first stage of fatigue damage, and thus the fibres with good orientation can help resist crack or restrain its growth.

Generally, there is no precise standard illustrating the exact failure probability that should be used for the design considering the aspect of fatigue failure [70]. To ensure a conservative and reliable fatigue design, 5% is considered as a limit of the failure probability [70], while Goel and Singh [10] mentioned that the predicted fatigue life corresponding to the lowest failure probability should be selected for the design. Thus, the S-N<sub>p</sub> relationship of all mixtures at the failure probability of 0.05 is illustrated in **Fig. 15**. It can be seen that the predicted life (in terms of logarithm form) were quite close when the stress level was the highest (i.e. 0.90), while the differences between each mixture generally increased with decreasing stress level. For instance, when the stress level was 0.75, the differences between each mixture were quite distinct. The predicted fatigue life of RTPPF12, RTPPF24, RTPPF48 and RTPPF96 was improved by 21.8%, 41.4%, 55.7% and 37.5%, respectively compared to that of F0. RTPPF48 achieved the highest fatigue life, which in turn suggests that the fibre orientation of RTPPF48 at the cracking surface is more appropriate (mostly perpendicular) and the teeny amount of crumb rubber (i.e. 2.07 kg/m<sup>3</sup>) may absorb some energy whist loading. As shown in **Fig. 15**, further addition of RTPPF (i.e. 9.6 kg/m<sup>3</sup>) slightly weakened the positive influence on fatigue performance of concrete (i.e. the position of the fitted line for RTPPF96 was generally lower), which can be primarily attributed to the poor workability (lower compactness) and inappropriate fibre distribution (poorer internal structure of FRC) [40] showing good consistence with the results of compressive and flexural strengths. On the other hand, PPF09 presented longer fatigue life (in terms of logarithm form) than RTPPF24 at the low stress level (about 6.1% higher), but the difference dropped gradually with

increasing stress level. When the stress level was 0.80, the fatigue life of PPF09 was even smaller than that of RTPF24 (9.3% lower). As observed, RTPF48 consistently demonstrated longer fatigue life than that of PPF09 implying that, the appropriate fibre content regarding this aspect is 4.8 kg/m<sup>3</sup>.

It was reported that reliable fatigue equations can be applied by engineers to estimate the expected flexural fatigue strength of a specific concrete mixture [8]. Accordingly, in this work, a double-logarithm fatigue equation was developed for each mixture under different failure probabilities within the following boundary conditions:

$$\begin{cases} \text{When } N = 1, S = 1 \\ \text{When } N \rightarrow \infty, S \rightarrow 0 \end{cases}$$

The developed fatigue functions for all mixtures under various failure probabilities with the corresponding correlation coefficient ( $r$ ) are listed in **Table 6**. The value of  $r$  of each equation ranged from 0.8370 to 0.9877 (mostly larger than 0.9) indicating that the fatigue equations developed in this study are reliable to be used to predict the flexural fatigue performance for a concrete mixture.

#### 3.3.4 Evolution of fatigue damage

As discussed in Section 3.2.1, fatigue damage process mainly consists of three main stages [20, 62]. By monitoring the change of strain against the cycle ratio (see **Fig. 16**), three stages could be demonstrated. The curves in **Fig. 16** are also known as cyclic creep curve [28]. With respect to the cycle ratio, it is defined as the ratio of the number of cycles whilst fatigue loading to the total number of cycles up to the final failure of concrete. Ideally, all mixtures should exhibit a similar trend that the strain increased gradually with a slight change of cycle ratio in the first stage (i.e. initiation of microcracks), while in the second stage, the strain changed at a constant rate (i.e. steady crack propagation along with increasing formation of microcracks). Finally, the strain ascended dramatically up to the final failure point (i.e. combined development of microcracks and macrocracks) [71]. It is worth noting that the second stage accounts for most of the service life of concrete [71] suggesting that the secondary strain rate is essential for the fatigue life of concrete. As shown in **Fig. 16**, most of the curves are consistent to the fatigue damage process mentioned previously. However, a slight change of tendency in the second stage was observed under a certain stress level. For instance, the secondary strain rate of F0 was slightly decreased at the end of the second stage when the stress level was 0.85 (see **Fig. 16a**), which could be associated with the concrete age and stress distribution during the fatigue testing [71]. For FRC, similar phenomenon can be also observed, which could be

attributed to the fibre bridging effect. With the addition of fibres, the development of cracks is limited leading to decreased strain rate. Nevertheless, the fibre effectiveness was not pronounced in the second stage. Thus, the secondary strain rates of all FRCs were constant at different stress levels. In addition, for all mixtures, it can be seen that the strain at a high stress level was larger than that at a low stress level, which in turn suggests that the fatigue damage at higher stress level was more severe. However, different from concrete mixture without fibre reinforcement, the cycle ratio of FRC at the end of first stage was normally larger implying that the fibre incorporation prolonged the first stage of fatigue damage. This is primarily ascribed to the fibre bridging action with the presence of microcracks (i.e. restrain the growth of microcracks) and thereby, more energy is absorbed by the fibres at the cracking zone through stress transfer mechanism [4, 72]. Due to the action of fibres, the fatigue damage is delayed leading to the extended duration of first-stage fatigue damage.

Generally, the cycle ratio at the end of first stage is denoted as  $k_1$ , while the cycle ratio at the beginning of third stage is regarded as  $k_2$ . The cycle ratio in different stages for all mixtures under various stress levels is quantified and presented in [Fig. 17](#). As discussed in the previous study [21],  $k_1$  and  $k_2$  of plain concrete was around 0.1 and 0.9, respectively. In this study, the corresponding value of  $k_1$  and  $k_2$  for F0 was ranging from 0.08 to 0.13 and 0.87 to 0.93 respectively under different stress levels. For RTPF-FRC, the values of  $k_1$  were generally higher than that of F0 at all stress levels (i.e. 0.12-0.14 for RTPF12; 0.13-0.15 for RTPF24 and RTPF48; 0.12-0.14 for RTPF96), which supports previous discussion that the addition of fibres prolongs the first stage of fatigue damage. However, the values of  $k_2$  of all RTPF-FRC in this study were similar to that of F0, which shows similarity with a previous study [20] that carbon-FRC exhibited almost constant value of  $k_2$  in comparison with plain concrete mixture. This can be attributed to the lost effectiveness of fibres during the second stage. As mentioned before, the main mechanism of the second stage is steady crack propagation with the continuous formation of microcracks simultaneously. RTPF is efficient in restraining the growth of microcracks at the early age, but gradually lost effectiveness when the cracks propagate (to larger size) [40]. After several cycles of loading, RTPF across the fracture zone may be pulled out or ruptured mostly during the first stage of loading [5]. On the other hand, similar results were observed for PPF09. RTPF24 and RTPF48 exhibited comparable performance with PPF09 considering the effect of delaying the fatigue damage of concrete during the first stage. For instance, when the stress ratio was 0.80, the values of  $k_2$  for RTPF24 and RTPF48 were 0.15, which was slightly higher than

that of PPF09 (i.e. 0.14).

Regarding the fatigue failure modes of all mixtures, no prominent difference was recognized, which showed a general phenomenon that, independent of fibre content, concrete mixture reinforced with either RTPF or PPF was split into half illustrating a single macrocrack (see [Fig. 18](#)). This observation is in good agreement with Li et al. [5] that the static compressive failure pattern of FRC was similar to its fatigue failure mode after compressive failure. The reason could be ascribed to the insufficient load-carrying capacity of RTPF- or PPF-FRC under repetitive cyclic loading implying that either RTPF or PPF could not effectively bridge the crack after several loading cycles. As shown in [Table 2](#), RTPF and PPF have relatively lower strength and stiffness, which largely hinder their bridging efficiencies when the loading cycle and crack size become larger. In terms of the SEM images, [Fig. 19](#) illustrates the surface condition of RTPF within the matrix after the fatigue failure. As seen in [Fig. 19a](#), RTPFs were found to be pulled out and a clear ruptured end was identified, which implies that RTPFs bridging the microcracks are pulled out after several cycles of loading mainly within the first stage of fatigue damage. The damage condition of RTPF shown in [Fig. 19b](#) was more severe (a serious broken surface was observed), which could be attributed to the continuous damage after the fibre is pulled out or ruptured. In addition, the trace of friction observed in [Fig. 19a](#) could provide the evidence that when the fibre is pulled out, it suffers from increasing cycles of loading (mainly after the first stage of fatigue damage) and friction with the matrix [5]. Consequently, these combined actions result in severe damage on RTPF. By contrast, as seen in [Fig. 20a](#), similarly, PPF was pulled out or ruptured where a long fibre channel appeared on the concrete matrix. PPFs were also damaged seriously, which could be ascribed to the continuous pulling (on the tension side of the specimen) or crushing (on the compression side of the specimen) caused by the external loading. Moreover, as shown in [Fig. 20b](#), scratch or broken line can be identified on the surface of PPF, which supports previous discussion about the continuous damage on fibre. To sum up, the fatigue failure mechanism is similar for both RTPF- and PPF-FRC that most of the fibres are pulled out or ruptured within the first-stage fatigue damage due to lower strength or stiffness, or shorter length and afterwards, fibres remaining in the cracking zone may experience uninterrupted pulling or crushing forces due to the repetitive cyclic loading. By comparing [Fig. 19b](#) and [Fig. 20b](#) (magnification: 800x), the damage condition of RTPF was more severe than that of PPF. As discussed in Section 3.2.1, RTPF24 and RTPF48 generally had longer fatigue life than PPF09 noting that RTPF within the matrix

experiences more cycles of loading prior to the final failure. The number of fibres within the matrix increases with increasing fibre volume fraction. Moreover, due to the shorter length of RTPF, the fibre spacing is relatively smaller [60]. Thus, the bridging efficiency at a single microcrack within the matrix would be increased (i.e. more fibres are around one individual crack) and consequently, the tensile capacity of the whole composite enhances contributing to the improvement in its fatigue behaviour. During fatigue loading, for a specific microcrack, part of the fibres bridges the crack, while the pulled-out or ruptured fibres nearby continue to experience the forces caused by the external loading resulting in severe damage condition, as shown in [Fig. 19b](#).

Although the damage condition of RTPF after fatigue loading was serious, it still contributes to the improved fatigue behaviour owing to the early-age bridging action, and increased fracture energy and frictional force (with the presence of appropriate amount of rubber particles). Additionally, under the same fibre volume fraction (0.1%  $V_f$ ), the flexural strength, fatigue behaviour and dynamic properties exhibited by RTPF12 were relatively poorer than those of PPF09. Thus, it is recommended that PPF should be replaced by higher volume fraction of RTPF to ensure better static, dynamic and fatigue performance.

#### **4. Conclusions**

This study experimentally investigated the flexural fatigue performance of concrete reinforced with recycled tyre polymer fibre (RTPF) considering different fibre dosages (i.e., 1.2, 2.4, 4.8 and 9.6  $\text{kg/m}^3$  corresponding to 0.1%, 0.2%, 0.4% and 0.8%  $V_f$ ) and various stress levels (i.e.,  $S = 0.90, 0.85, 0.80$  and  $0.75$ ). The results were compared with those without fibre incorporation and with the addition of 0.9  $\text{kg/m}^3$  (i.e. 0.1%  $V_f$ ) of polypropylene fibre (PPF). Based on the results in this study, the main conclusions can be drawn as follows:

- Concrete mixture reinforced with RTPF exhibited better ultimate flexural strength than that without fibre reinforcement (enhanced by 3.6-9.6%). However, the workability and compressive strength decreased with increasing RTPF content. The rubber granules attached the RTPFs contributed to the increase of air content in fresh FRC.
- The fatigue life of all mixtures in this study followed the two-parameter Weibull distribution under different stress levels. The developed double-logarithm fatigue equations can be used to well describe the relationship between fatigue life and applied stress level of all mixtures with high correlation coefficients ranging from 0.8370 to 0.9877 considering different failure probabilities

(i.e., 0.05, 0.10, 0.20, 0.30, 0.40 and 0.50).

- The overall fatigue performance of concrete was enhanced by incorporating a suitable amount of RTPF. In comparison with the predicted fatigue life of reference mixture, the most predicted life increments (in terms of logarithm form) of RTPF12, RTPF24, RTPF48, RTPF96, PPF09 ranged from 3.3-25.1%, 32.5-49.9%, 22.9-58.3%, 6.6-37.5% and 13.5-50.0%) respectively under various failure probabilities. Considering workability, compressive strength, flexural strength and fatigue behaviour, the appropriate RTPF content in FRC is in the range of 2.4-4.8 kg/m<sup>3</sup> (i.e. 0.2-0.4%  $V_f$ ).
- The fatigue failure mechanisms of RTPF and PPF reinforced concrete were similar consisting of three main stages. Both RTPF and PPF may continuously experience pulling and crushing forces or friction with the matrix when they are pulled out or ruptured. By considering static, dynamic and fatigue performance, 0.1%  $V_f$  of PPF could be substituted by 0.2-0.4%  $V_f$  of RTPF in FRC.

This paper investigated the overall flexural fatigue performance of concrete mixture reinforced with RTPF considering different stress levels and fibre contents, whereas the probabilistic fatigue model was not developed. Given the fact that the number of performed fatigue test would potentially affect the corresponding fatigue results, more samples should be prepared for each mixture and the effect of fatigue loading frequency on the fatigue performance should be considered in order to develop an accurate fatigue model towards a comprehensive understanding of the fatigue behaviour of RTPF-FRC. Considering the static flexural strength, maximum fatigue stress, minimum stress below which no fatigue failure will arise, and fatigue loading frequency, the fatigue results of RTPF-FRC can be used to validate or improve the compressive fatigue model developed by Saucedo et al. [28]. This is a subject of ongoing work and will be presented in a future publication.

### **Acknowledgement**

The authors gratefully acknowledge the financial support of the Engineering and Physical Sciences Research Council (EPSRC), United Kingdom via grant EP/R041504/1 “Development of a Novel Self-Healing Composite for Sustainable and Resilient Concrete Infrastructure”, the State Key Laboratory of Silicate Materials for Architectures (Wuhan University of Technology) (No. SYSJJ2017-08 and No. SYSJJ2018-08), Research Fund of Liaoning Natural Science Foundation (No. 20170540304 and No. 20170540303), National Training Program of Innovation and Entrepreneurship for Undergraduates (No. 201810145047) and Fundamental Research Funds for the Central

Universities (No. N170104023).

## References

- [1] N. Buratti, C. Mazzotti, M. Savoia, Post-cracking behaviour of steel and macro-synthetic fibre-reinforced concretes, *Construction and Building Materials* 25(5) (2011) 2713-2722.
- [2] J.O. Lerch, H.L. Bester, A.S. Van Rooyen, R. Combrinck, W.I. de Villiers, W.P. Boshoff, The effect of mixing on the performance of macro synthetic fibre reinforced concrete, *Cement and Concrete Research* 103 (2018) 130-139.
- [3] E.V. Sarmiento, M.R. Geiker, T. Kanstad, Influence of fibre configuration on the mechanical behaviour of standard test specimens and full-scale beams made of flowable FRC, *Construction and Building Materials* 111 (2016) 794-804.
- [4] M.K. Lee, B.I.G. Barr, An overview of the fatigue behaviour of plain and fibre reinforced concrete, *Cement and Concrete Composites* 26(4) (2004) 299-305.
- [5] Q. Li, B. Huang, S. Xu, B. Zhou, R.C. Yu, Compressive fatigue damage and failure mechanism of fiber reinforced cementitious material with high ductility, *Cement and Concrete Research* 90 (2016) 174-183.
- [6] A. Amin, S.J. Foster, R.I. Gilbert, W. Kaufmann, Material characterisation of macro synthetic fibre reinforced concrete, *Cement and Concrete Composites* 84 (2017) 124-133.
- [7] T. Plagué, C. Desmettre, J.P. Charron, Influence of fiber type and fiber orientation on cracking and permeability of reinforced concrete under tensile loading, *Cement and Concrete Research* 94 (2017) 59-70.
- [8] S.P. Singh, S.K. Kaushik, Fatigue strength of steel fibre reinforced concrete in flexure, *Cement and Concrete Composites* 25(7) (2003) 779-786.
- [9] H. Hacène, B. Ghofrane, D. Gérard, Flexural fatigue performance of metal steel fibre reinforced mortar – Influence of fibre aspect ratio and type, *Construction and Building Materials* 58 (2014) 166-170.
- [10] S. Goel, S.P. Singh, Fatigue performance of plain and steel fibre reinforced self compacting concrete using S–N relationship, *Engineering Structures* 74 (2014) 65-73.
- [11] E. Poveda, G. Ruiz, H. Cifuentes, R.C. Yu, X. Zhang, Influence of the fiber content on the compressive low-cycle fatigue behavior of self-compacting SFRC, *Int. J. Fatigue* 101 (2017) 9-17.
- [12] J. Zhang, H. Stang, V.C. Li, Fatigue life prediction of fiber reinforced concrete under flexural

load, *Int. J. Fatigue* 21(10) (1999) 1033-1049.

[13] J. Wang, C. Li, X. Fan, M. Zhang, Flexural fatigue behavior of layered hybrid fiber reinforced concrete, *Journal of Wuhan University of Technology-Mater. Sci. Ed.* 22(3) (2007) 560-563.

[14] Z. Sun, Q. Xu, Microscopic, physical and mechanical analysis of polypropylene fiber reinforced concrete, *Materials Science and Engineering: A* 527(1) (2009) 198-204.

[15] M.R. Mohamadi, J.A. Mohandesi, M. Homayonifar, Fatigue behavior of polypropylene fiber reinforced concrete under constant and variable amplitude loading, *Journal of Composite Materials* 47(26) (2012) 3331-3342.

[16] M. Mulheron, J.T. Kevern, T.D. Rupnow, Laboratory Fatigue and Toughness Evaluation of Fiber-Reinforced Concrete, *Transportation Research Record: Journal of the Transportation Research Board* 2508 (2015) 39-47.

[17] A. Medeiros, X. Zhang, G. Ruiz, R.C. Yu, M.d.S.L. Velasco, Effect of the loading frequency on the compressive fatigue behavior of plain and fiber reinforced concrete, *Int. J. Fatigue* 70 (2015) 342-350.

[18] J. Qiu, X.-N. Lim, E.-H. Yang, Fatigue-induced deterioration of the interface between micro-polyvinyl alcohol (PVA) fiber and cement matrix, *Cement and Concrete Research* 90 (2016) 127-136.

[19] S.-J. Choi, J.-S. Mun, K.-H. Yang, S.-J. Kim, Compressive fatigue performance of fiber-reinforced lightweight concrete with high-volume supplementary cementitious materials, *Cement and Concrete Composites* 73 (2016) 89-97.

[20] Z. Deng, The fracture and fatigue performance in flexure of carbon fiber reinforced concrete, *Cement and Concrete Composites* 27(1) (2005) 131-140.

[21] W. Wang, S. Wu, H. Dai, Fatigue behavior and life prediction of carbon fiber reinforced concrete under cyclic flexural loading, *Materials Science and Engineering: A* 434(1) (2006) 347-351.

[22] X. Chen, Z. Liu, S. Guo, Y. Huang, W. Xu, Experimental study on fatigue properties of normal and rubberized self-compacting concrete under bending, *Construction and Building Materials* 205 (2019) 10-20.

[23] Y. Mohammadi, S.K. Kaushik, Flexural fatigue-life distributions of plain and fibrous concrete at various stress levels, *Journal of materials in Civil Engineering-ASCE* 17(6) (2005) 650-8.

[24] S.P. Singh, Y. Mohammadi, S. Goel, S.K. Kaushik, Prediction of Mean and Design Fatigue Lives of Steel Fibrous Concrete Beams in Flexure, *Adv. Struct. Eng* 10(1) (2007) 25-36.

- [25] G. Kaur, S.P. Singh, S.K. Kaushik, Influence of mineral additions on flexural fatigue performance of steel fibre reinforced concrete, *Materials and Structures* 49(10) (2016) 4101-4111.
- [26] Y. Lv, H.-m. Cheng, Z.-g. Ma, Fatigue performances of glass fiber reinforced concrete in flexure, *Procedia Engineering* 31 (2012) 550-556.
- [27] E. Castillo, A. Fernández-Canteli, *A Unified Statistical Methodology for Modeling Fatigue Damage*, Springer 2009.
- [28] L. Saucedo, R.C. Yu, A. Medeiros, X. Zhang, G. Ruiz, A probabilistic fatigue model based on the initial distribution to consider frequency effect in plain and fiber reinforced concrete, *Int. J. Fatigue* 48 (2013) 308-318.
- [29] J.D. Ríos, H. Cifuentes, R.C. Yu, G. Ruiz, Probabilistic Flexural Fatigue in Plain and Fiber-Reinforced Concrete, *Materials (Basel)* 10(7) (2017) 767.
- [30] O. Onuaguluchi, N. Banthia, Scrap tire steel fiber as a substitute for commercial steel fiber in cement mortar: Engineering properties and cost-benefit analyses, *Resources, Conservation and Recycling* 134 (2018) 248-256.
- [31] K. Adalberth, Energy use during the life cycle of single-unit dwellings: Examples, *Build. Environ.* 32(4) (1997) 321-329.
- [32] H. Zhong, E.W. Poon, K. Chen, M. Zhang, Engineering properties of crumb rubber alkali-activated mortar reinforced with recycled steel fibres, *Journal of Cleaner Production* 238 (2019) 117950.
- [33] J.A.O. Barros, C. Frazão, A. Caggiano, P. Folino, E. Martinelli, H. Xargay, Z. Zamanzadeh, L. Lourenço, Cementitious Composites Reinforced with Recycled Fibres, in: J.A.O. Barros, L. Ferrara, E. Martinelli (Eds.), *Recent Advances on Green Concrete for Structural Purposes: The contribution of the EU-FP7 Project EnCoRe*, Springer International Publishing, Cham, 2017, pp. 141-195.
- [34] B.S. Thomas, R.C. Gupta, A comprehensive review on the applications of waste tire rubber in cement concrete, *Renewable and Sustainable Energy Reviews* 54 (2016) 1323-1333.
- [35] A. Baričević, M. Jelčić Rukavina, M. Pezer, N. Štirmer, Influence of recycled tire polymer fibers on concrete properties, *Cement and Concrete Composites* 91 (2018) 29-41.
- [36] A. Baricevic, M. Pezer, M. Jelcic Rukavina, M. Serdar, N. Stirmer, Effect of polymer fibers recycled from waste tires on properties of wet-sprayed concrete, *Construction and Building Materials* 176 (2018) 135-144.

- [37] M. Serdar, A. Baričević, M. Jelčić Rukavina, M. Pezer, D. Bjegović, N. Štirmer, Shrinkage Behaviour of Fibre Reinforced Concrete with Recycled Tyre Polymer Fibres, *International Journal of Polymer Science* 2015 (2015) 1-9.
- [38] S.-S. Huang, H. Angelakopoulos, K. Pilakoutas, I. Burgess, Reused tyre polymer fibre for fire-spalling mitigation, *Applications of Structural Fire Engineering*, 2015.
- [39] O. Onuaguluchi, N. Banthia, Durability performance of polymeric scrap tire fibers and its reinforced cement mortar, *Materials and Structures* 50(2) (2017).
- [40] M. Chen, W. Chen, H. Zhong, D. Chi, Y. Wang, M. Zhang, Experimental study on dynamic compressive behaviour of recycled tyre polymer fibre reinforced concrete, *Cement and Concrete Composites* 98 (2019) 95-112.
- [41] O. Onuaguluchi, N. Banthia, Value-added reuse of scrap tire polymeric fibers in cement-based structural applications, *Journal of Cleaner Production* 231 (2019) 543-555.
- [42] Synthetic fibres for cement, cement mortar and concrete, GB/T21120-2007, China, 2007.
- [43] Testing Methods of Workability of Normal Concrete, GB/T50080-2016, China Building Materials Academy, China, 2016.
- [44] Standard Test Method for Air Content of Freshly Mixed Concrete by the Pressure Method, ASTM C231-17a, ASTM International, West Conshohocken, PA, 2017.
- [45] Testing Methods of Mechanical Properties of Normal Concrete, GB/T50081-2002, China Building Materials Academy, China, 2002.
- [46] J.J. Ortega, G. Ruiz, R.C. Yu, N. Afanador-García, M. Tarifa, E. Poveda, X. Zhang, F. Evangelista, Number of tests and corresponding error in concrete fatigue, *Int. J. Fatigue* 116 (2018) 210-219.
- [47] H. Su, J. Yang, T.-C. Ling, G.S. Ghataora, S. Dirar, Properties of concrete prepared with waste tyre rubber particles of uniform and varying sizes, *Journal of Cleaner Production* 91 (2015) 288-296.
- [48] R. Si, S. Guo, Q. Dai, Durability performance of rubberized mortar and concrete with NaOH-Solution treated rubber particles, *Construction and Building Materials* 153 (2017) 496-505.
- [49] O. Onuaguluchi, N. Banthia, Long-term sulfate resistance of cementitious composites containing fine crumb rubber, *Cement and Concrete Composites* 104 (2019) 103354.
- [50] J. Wang, Q. Dai, R. Si, S. Guo, Mechanical, durability, and microstructural properties of macro synthetic polypropylene (PP) fiber-reinforced rubber concrete, *Journal of Cleaner Production* 234 (2019) 1351-1364.

- [51] A. Benazzouk, O. Douzane, K. Mezreb, M. Quéneudec, Physico-mechanical properties of aerated cement composites containing shredded rubber waste, *Cement and Concrete Composites* 28(7) (2006) 650-657.
- [52] F. Liu, W. Zheng, L. Li, W. Feng, G. Ning, Mechanical and fatigue performance of rubber concrete, *Construction and Building Materials* 47 (2013) 711-719.
- [53] L. Li, S. Ruan, L. Zeng, Mechanical properties and constitutive equations of concrete containing a low volume of tire rubber particles, *Construction and Building Materials* 70 (2014) 291-308.
- [54] L.-J. Li, Z.-Z. Chen, W.-F. Xie, F. Liu, Experimental study of recycled rubber-filled high-strength concrete, *Magazine of Concrete Research* 61(7) (2009) 549-556.
- [55] S. Ramdani, A. Guettala, M.L. Benmalek, J.B. Aguiar, Physical and mechanical performance of concrete made with waste rubber aggregate, glass powder and silica sand powder, *Journal of Building Engineering* 21 (2019) 302-311.
- [56] B. Zhou, Y. Uchida, Influence of flowability, casting time and formwork geometry on fiber orientation and mechanical properties of UHPFRC, *Cement and Concrete Research* 95 (2017) 164-177.
- [57] N. Yousefieh, A. Joshaghani, E. Hajibandeh, M. Shekarchi, Influence of fibers on drying shrinkage in restrained concrete, *Construction and Building Materials* 148 (2017) 833-845.
- [58] C. Fu, H. Ye, K. Wang, K. Zhu, C. He, Evolution of mechanical properties of steel fiber-reinforced rubberized concrete (FR-RC), *Composites Part B: Engineering* 160 (2019) 158-166.
- [59] B. Li, Y. Chi, L. Xu, Y. Shi, C. Li, Experimental investigation on the flexural behavior of steel-polypropylene hybrid fiber reinforced concrete, *Construction and Building Materials* 191 (2018) 80-94.
- [60] Z. Wu, C. Shi, W. He, D. Wang, Static and dynamic compressive properties of ultra-high performance concrete (UHPC) with hybrid steel fiber reinforcements, *Cement and Concrete Composites* 79 (2017) 148-157.
- [61] D.-Y. Yoo, N. Banthia, Mechanical properties of ultra-high-performance fiber-reinforced concrete: A review, *Cement and Concrete Composites* 73 (2016) 267-280.
- [62] C. Wang, Y. Zhang, Investigation into the fatigue damage process of rubberized concrete and plain concrete by AE analysis, *Journal of Materials in Civil Engineering* 23 (2011) 953-960.
- [63] R. Pacheco-Torres, E. Cerro-Prada, F. Escolano, F. Varela, Fatigue performance of waste rubber

concrete for rigid road pavements, *Construction and Building Materials* 176 (2018) 539-548.

[64] W. Weibull, CHAPTER IX - ANALYSIS OF RESULTS, in: W. Weibull (Ed.), *Fatigue Testing and Analysis of Results*, Pergamon 1961, pp. 184-249.

[65] K.M.A. Sohel, K. Al-Jabri, M.H. Zhang, J.Y.R. Liew, Flexural fatigue behavior of ultra-lightweight cement composite and high strength lightweight aggregate concrete, *Construction and Building Materials* 173 (2018) 90-100.

[66] K.-S. Yeon, Y.-S. Choi, K.-K. Kim, J.H. Yeon, Flexural fatigue life analysis of unsaturated polyester-methyl methacrylate polymer concrete, *Construction and Building Materials* 140 (2017) 336-343.

[67] O. Byung Hwan, Fatigue Analysis of Plain Concrete in Flexure, *Journal of structural engineering-ASCE* 112(2) (1986) 273-88.

[68] O. Byung Hwan, Fatigue Life Distributions of Concrete for Various Stress Levels, *Materials Journal* 88(2).

[69] O. AlShareedah, S. Nassiri, J.D. Dolan, Pervious concrete under flexural fatigue loading: Performance evaluation and model development, *Construction and Building Materials* 207 (2019) 17-27.

[70] A.G. Graeff, K. Pilakoutas, K. Neocleous, M.V.N.N. Peres, Fatigue resistance and cracking mechanism of concrete pavements reinforced with recycled steel fibres recovered from post-consumer tyres, *Engineering Structures* 45 (2012) 385-395.

[71] P.R. Sparks, J.B. Menzies, The effect of rate of loading upon the static and fatigue strengths of plain concrete in compression, *Magazine of Concrete Research* 25 (1973) 73-80.

[72] P.B. Cachim, J.A. Figueiras, P.A.A. Pereira, Fatigue behavior of fiber-reinforced concrete in compression, *Cement and Concrete Composites* 24(2) (2002) 211-217.

Figures

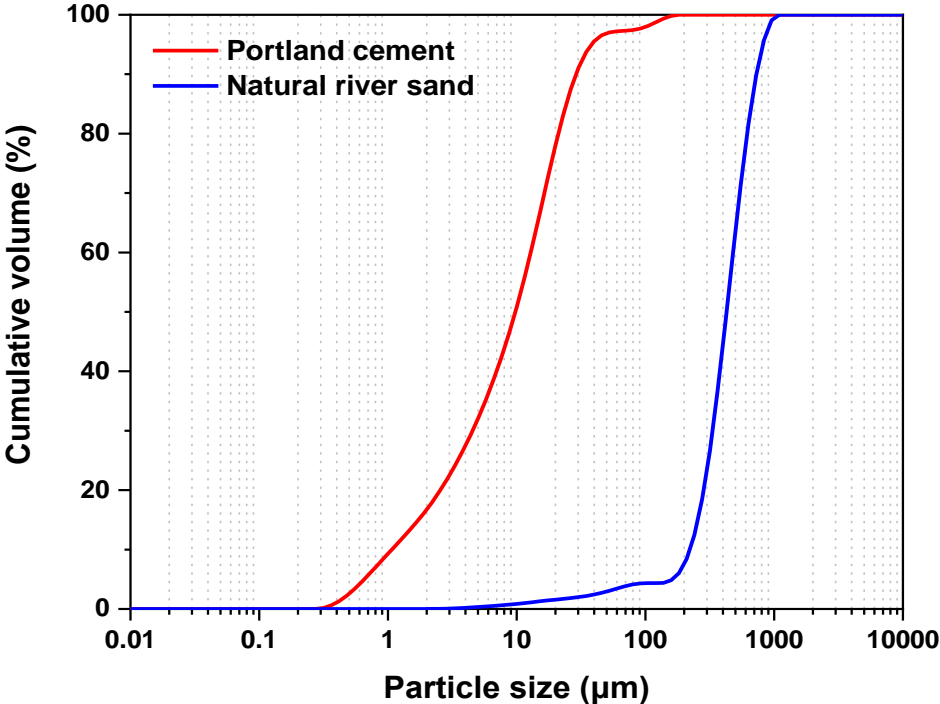
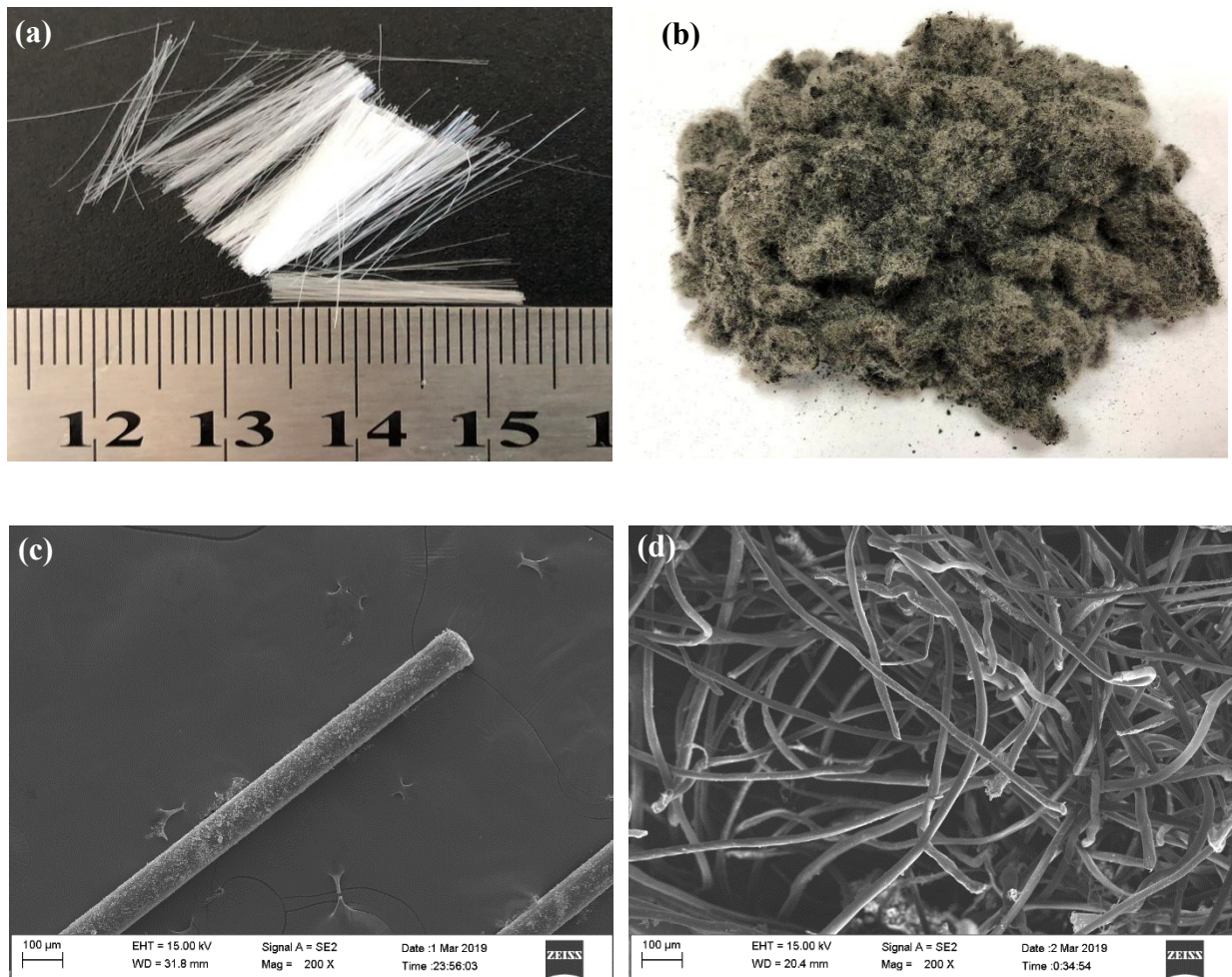


Fig. 1. Particle size distribution of cement and sand



**Fig. 2.** Fibres used in this study: (a) PPF; (b) RTPF (as-received RTPF with rubber granules attached); (c) SEM micrographs of PPF; (d) SEM micrographs of RTPF



**Fig. 3.** A schematic diagram showing the process of estimating the composition of RTPF

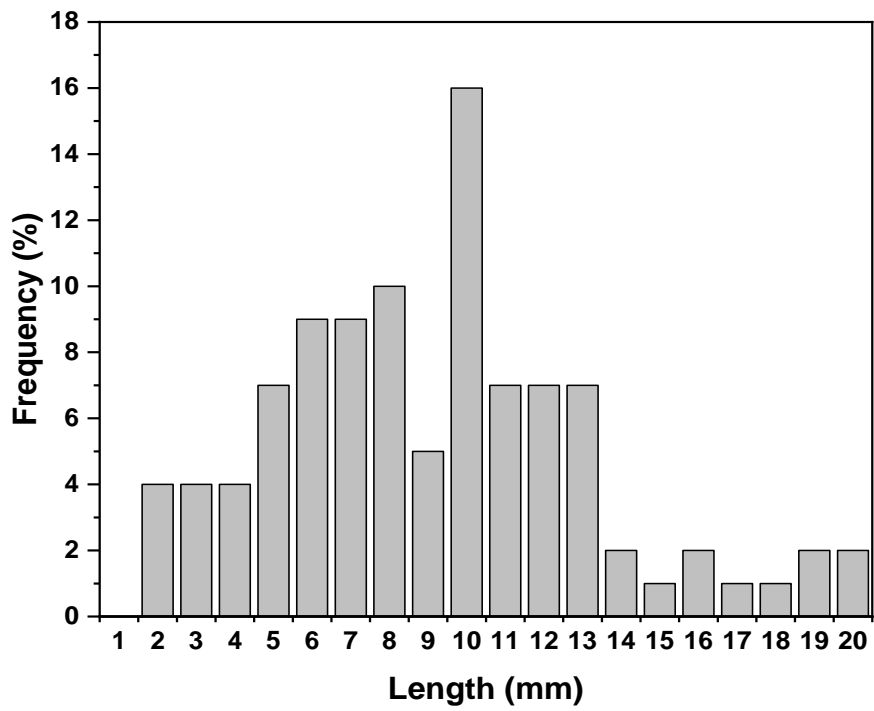


Fig. 4. Length distribution of RTPF

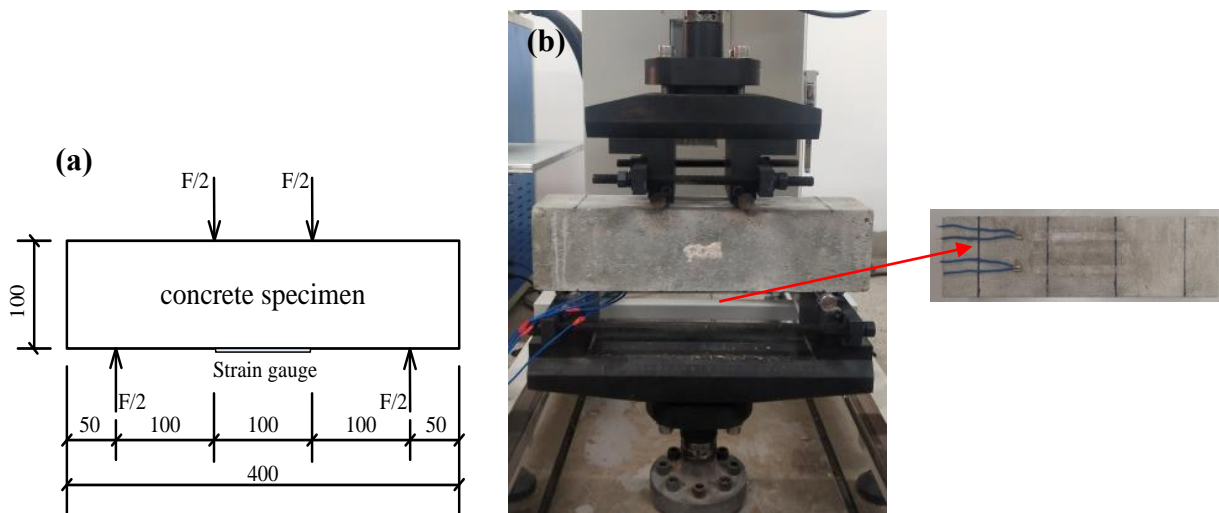
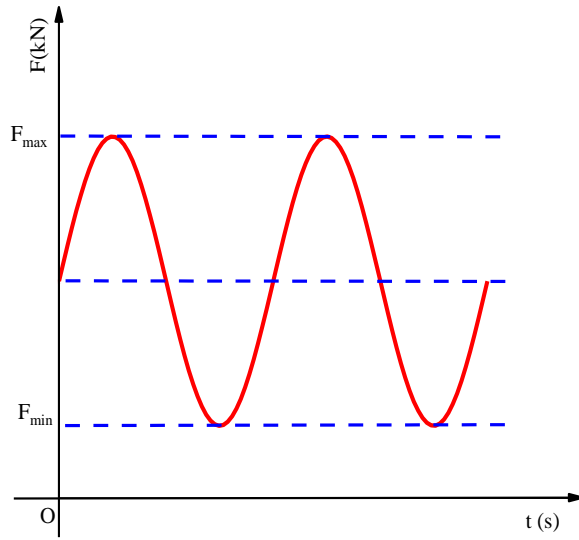
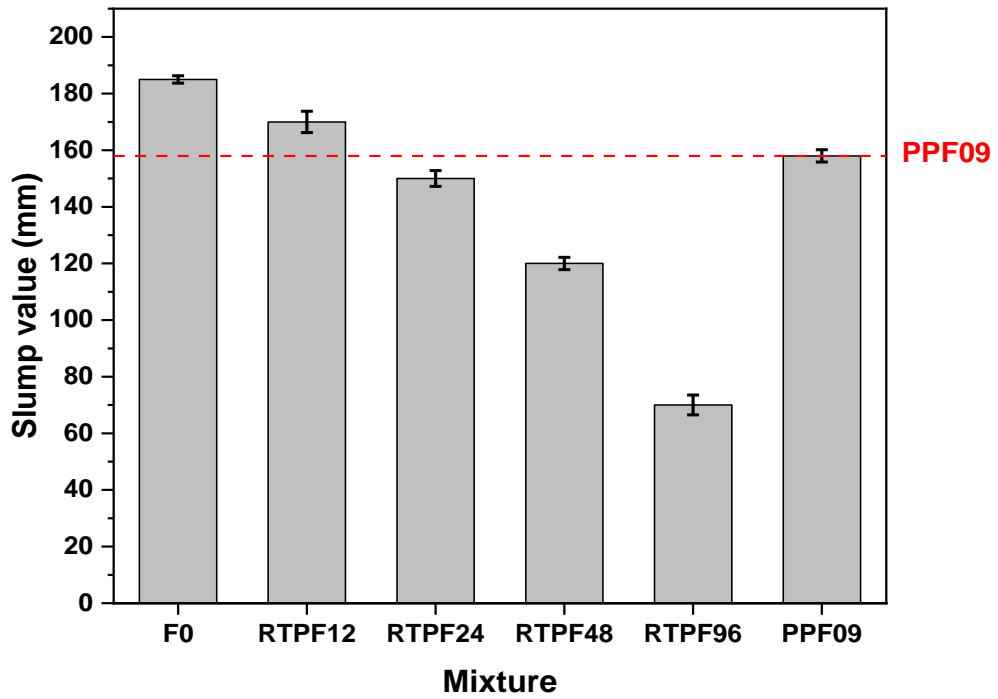


Fig. 5. Flexural loading test set-up: (a) schematic diagram; (b) picture



**Fig. 6.** Fatigue loading parameters (i.e.  $F_{max}$  &  $F_{min}$ )



**Fig. 7.** Slump value of all mixtures

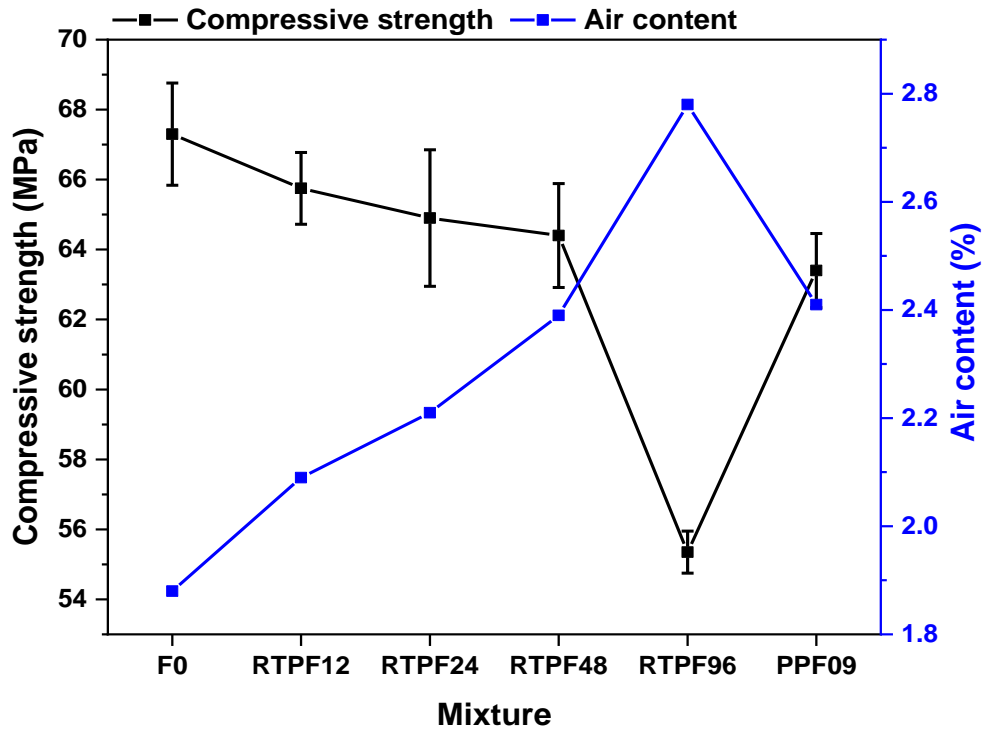


Fig. 8. Effects of fibre incorporation and air content on 28-d compressive strength of concrete

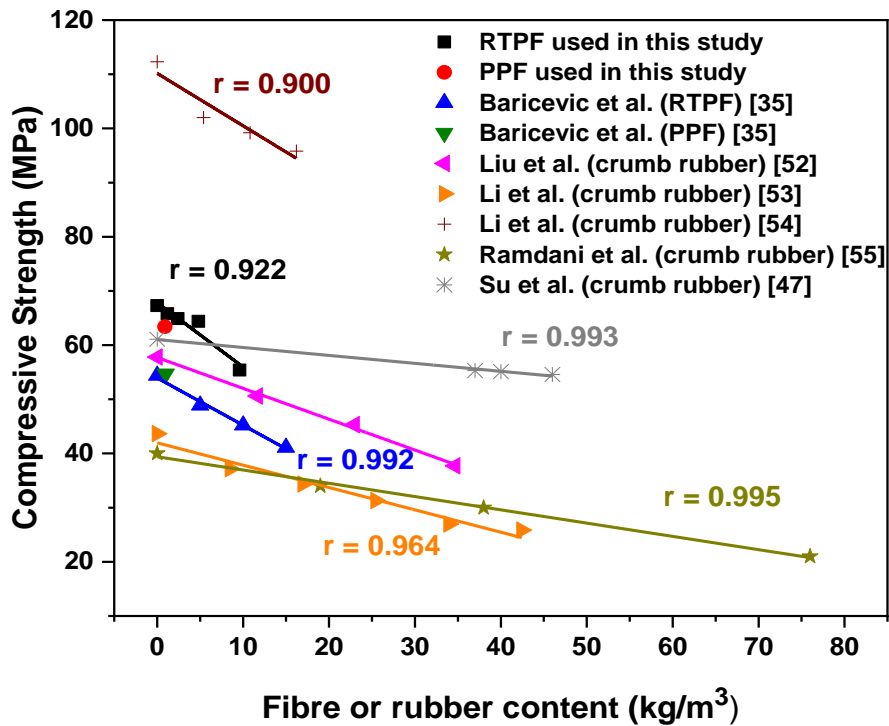


Fig. 9. Effect of RTPF (or PPF) or crumb rubber content on compressive strength of concrete

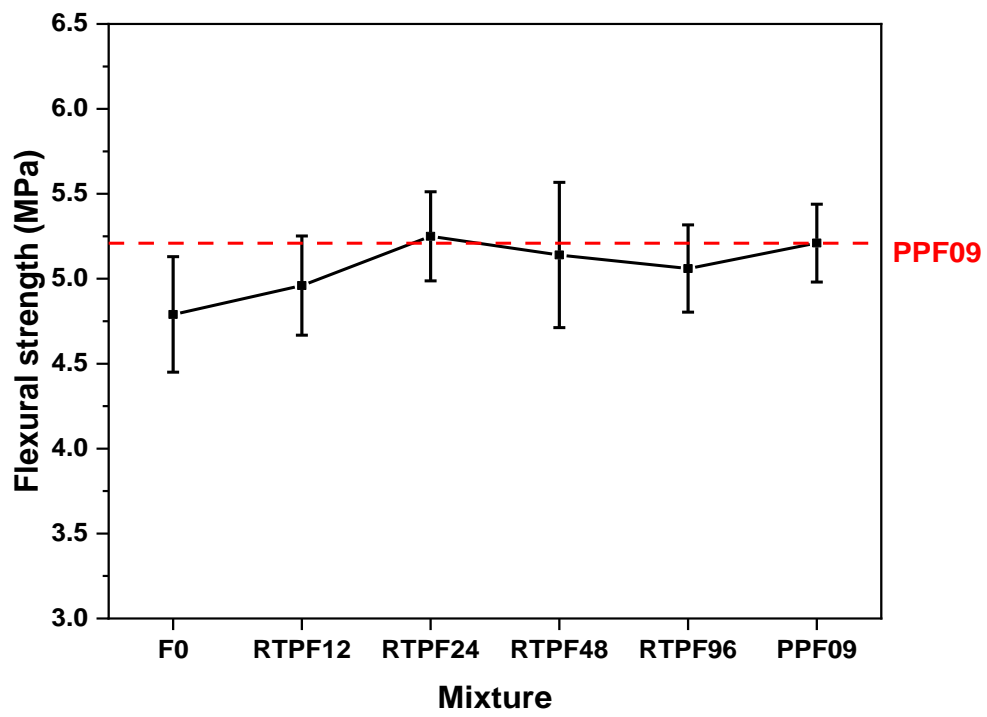


Fig. 10. 28-d flexural strength of all mixtures

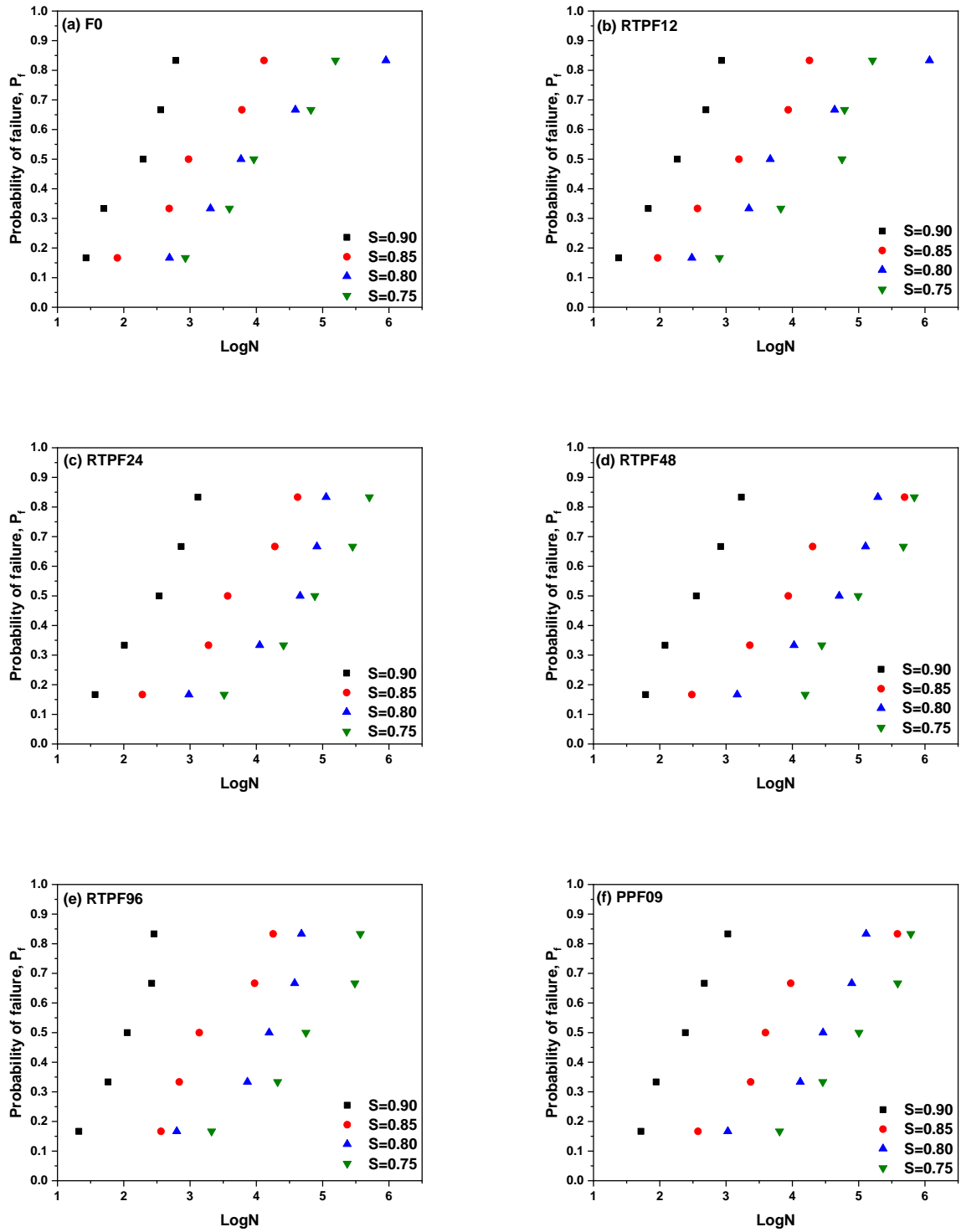
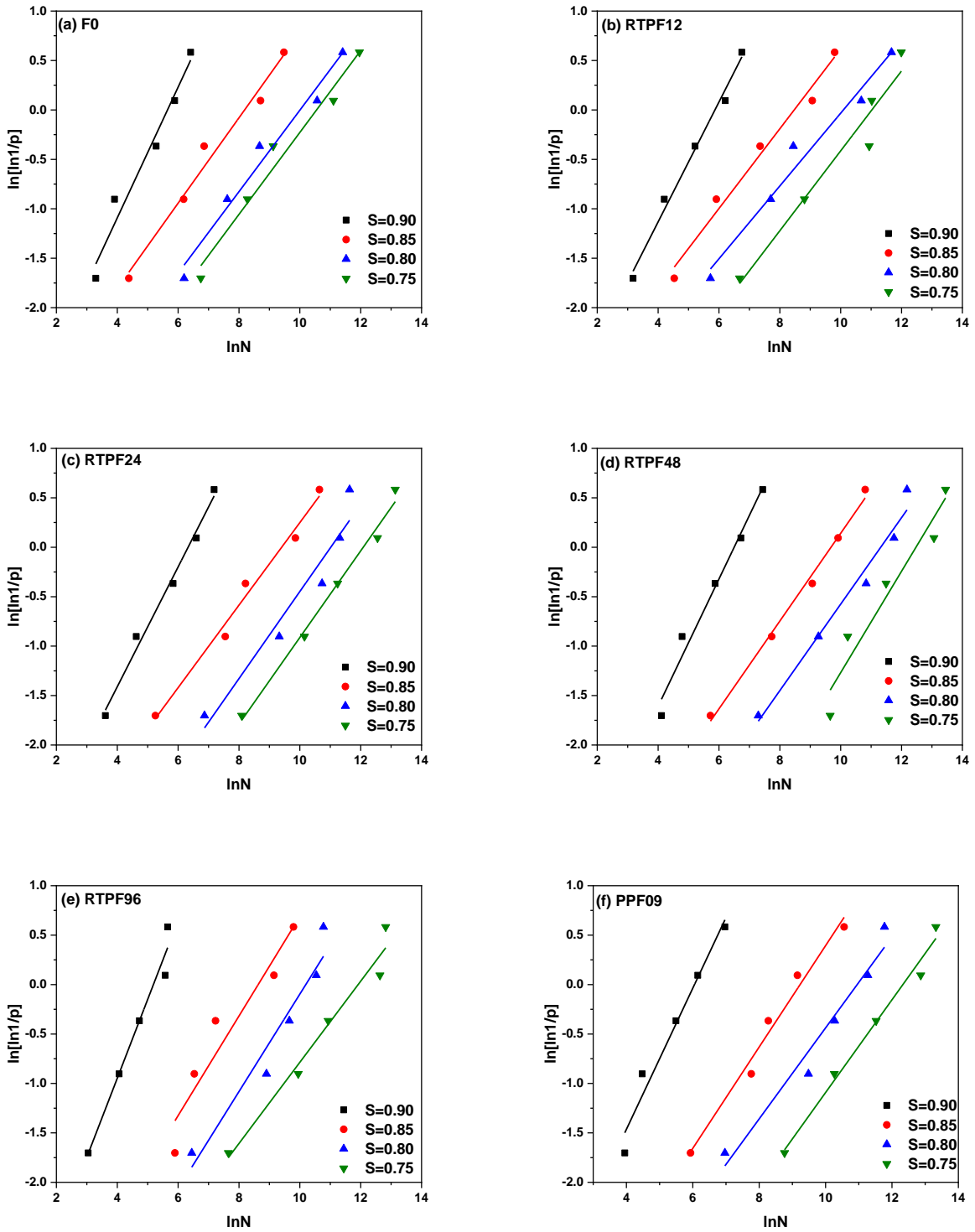
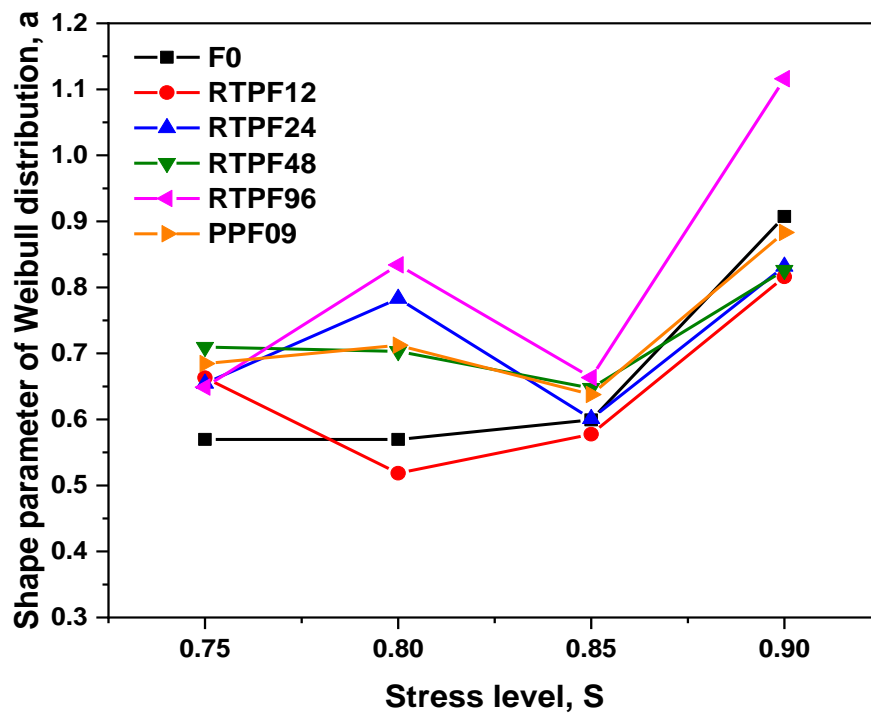


Fig. 11. Probability distribution of all mixtures



**Fig. 12.** Graphical analysis of fatigue life data for all mixtures



**Fig. 13.** Effect of stress level ( $S$ ) on shape parameter ( $a$ ) of the Weibull distribution

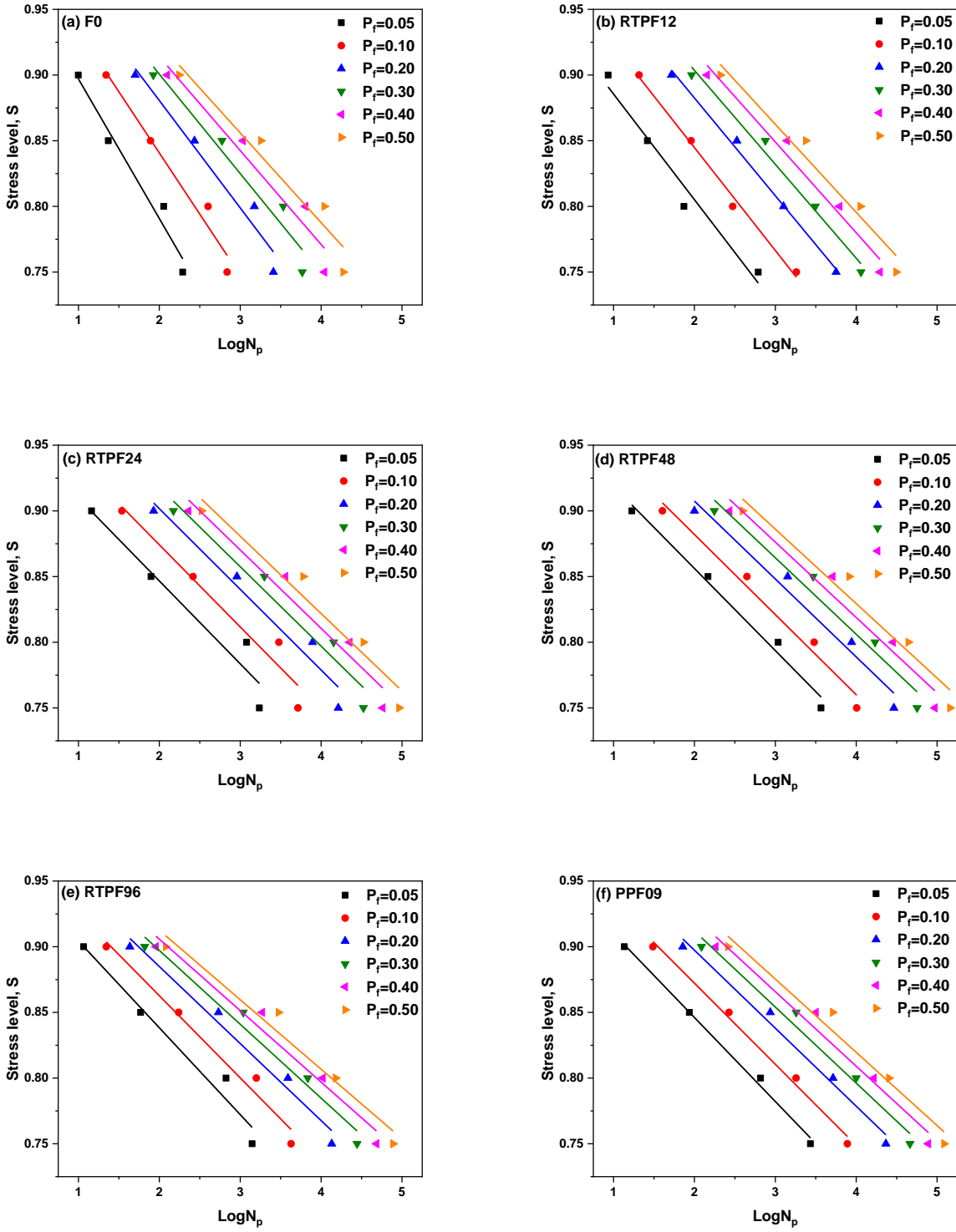
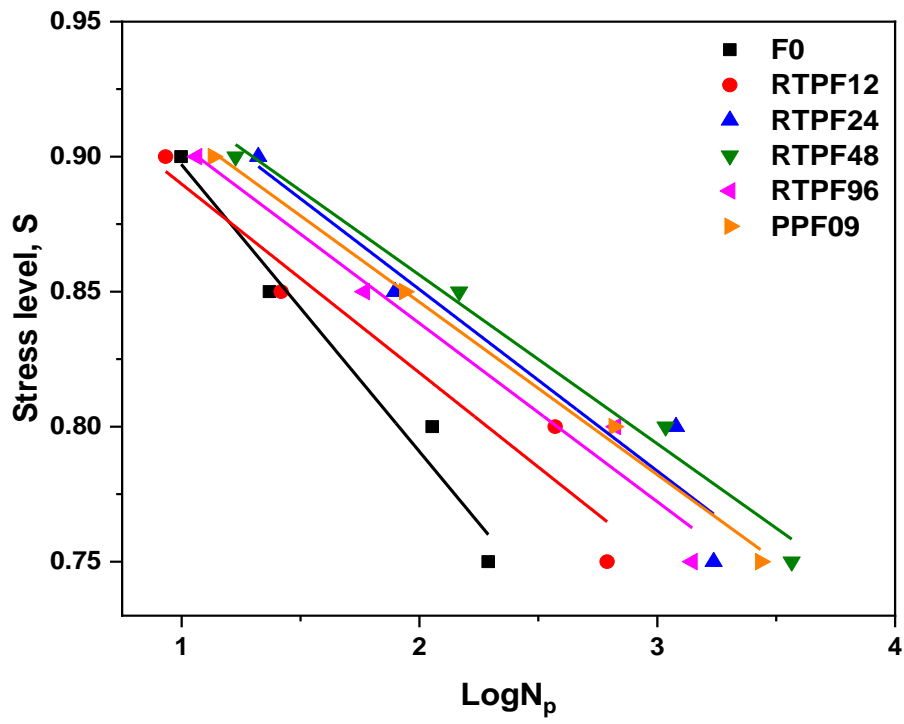


Fig. 14. S- $N_p$  relationship of all mixtures



**Fig. 15.** S-N<sub>p</sub> relationship of all mixtures when  $P_f = 0.05$

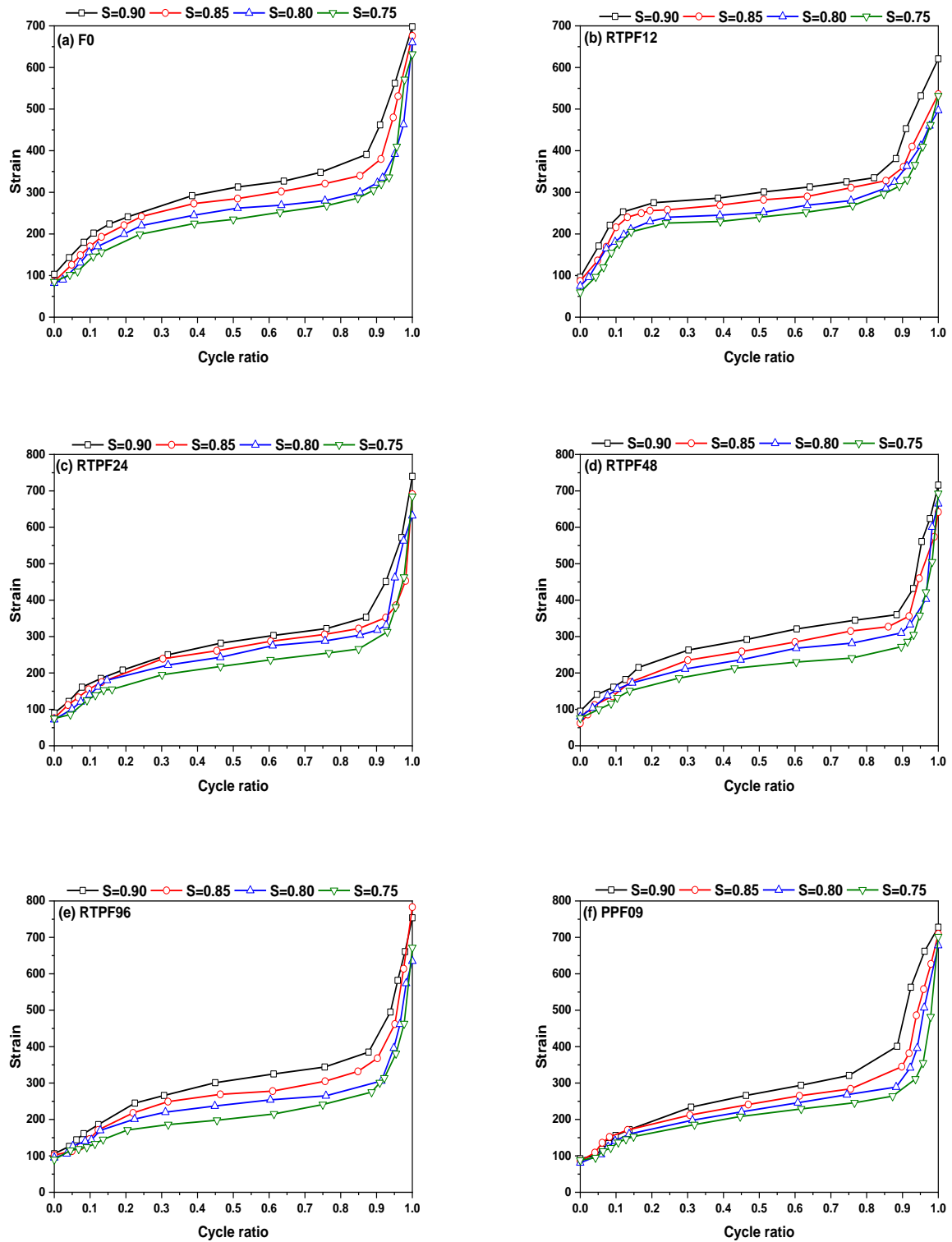
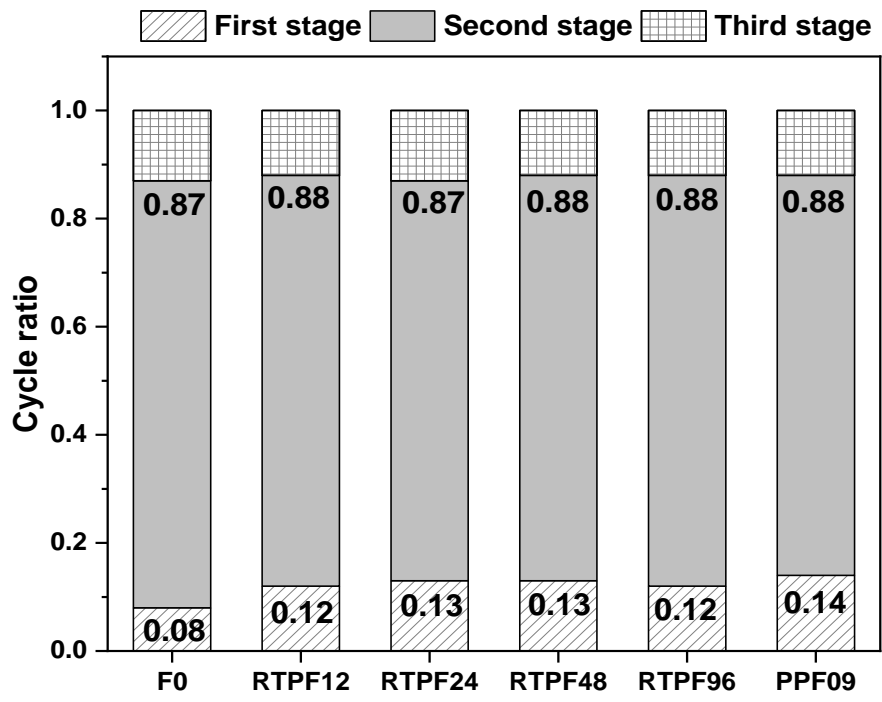
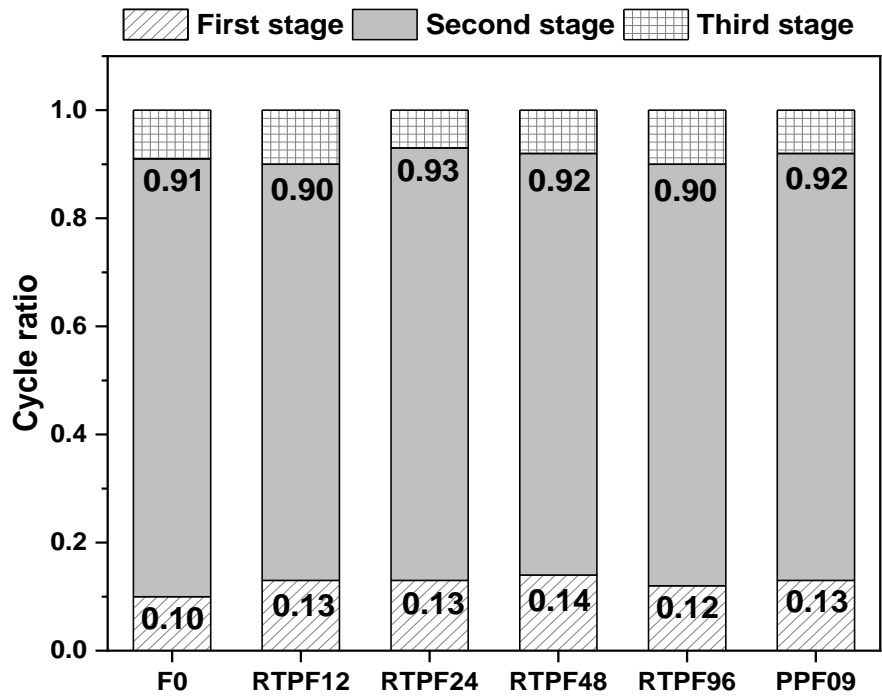


Fig. 16. Relationship between strain and cycle ratio for all mixtures under various stress ratios



(a) S=0.90



(b) S=0.85

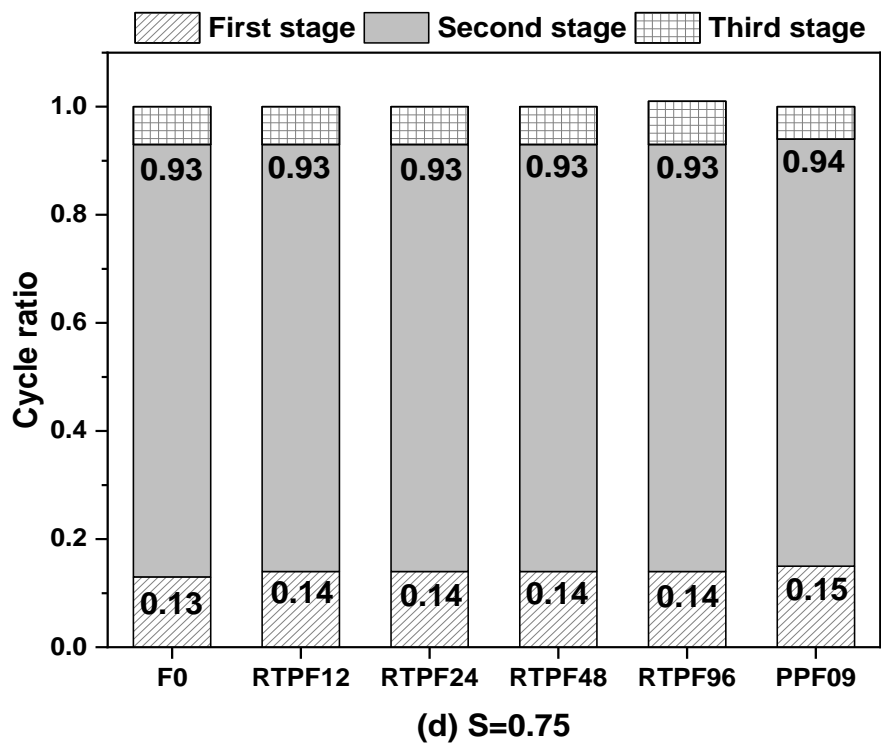
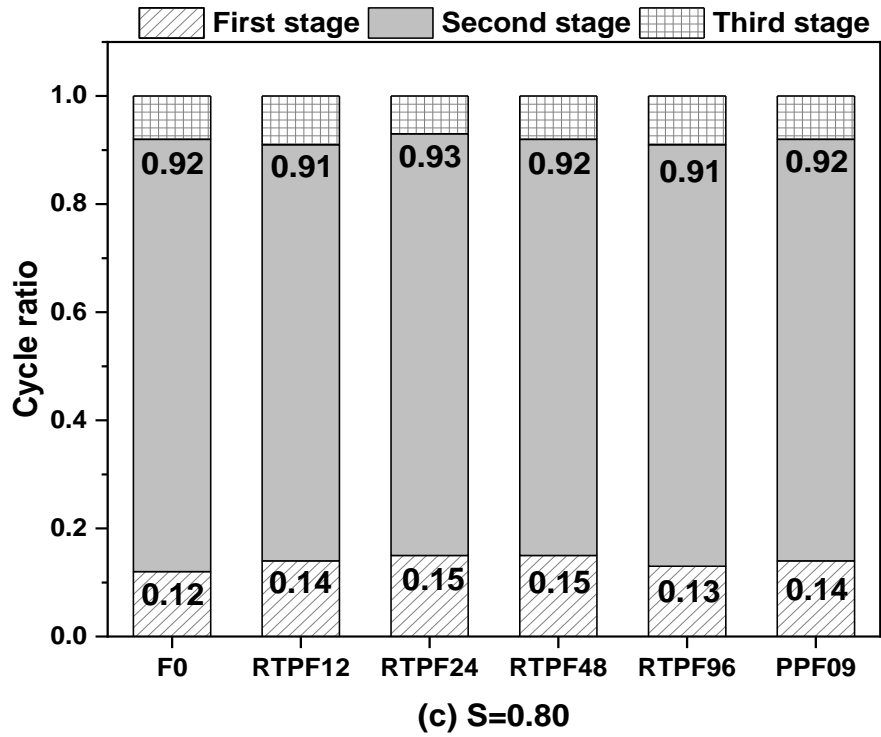
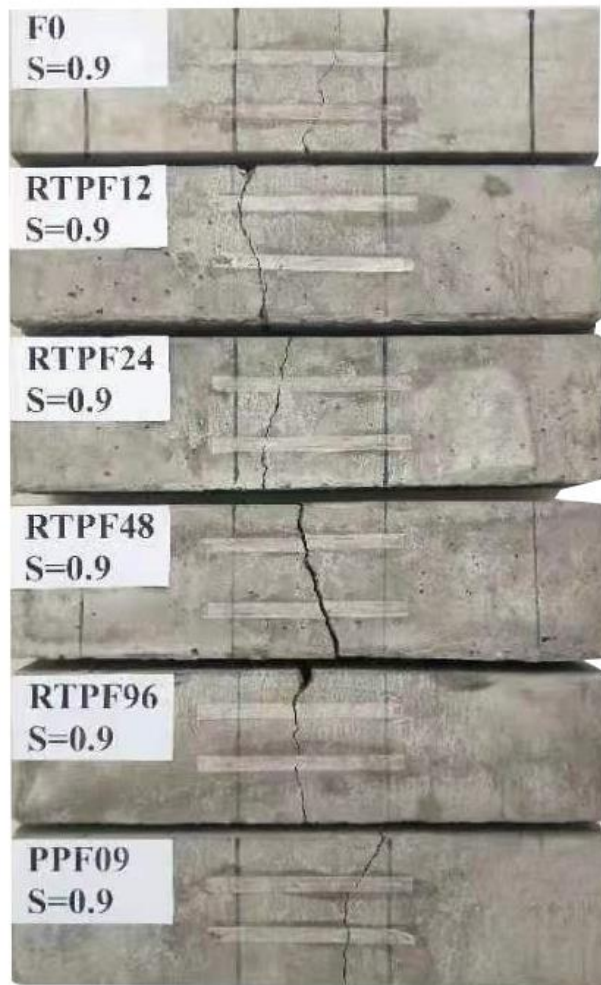
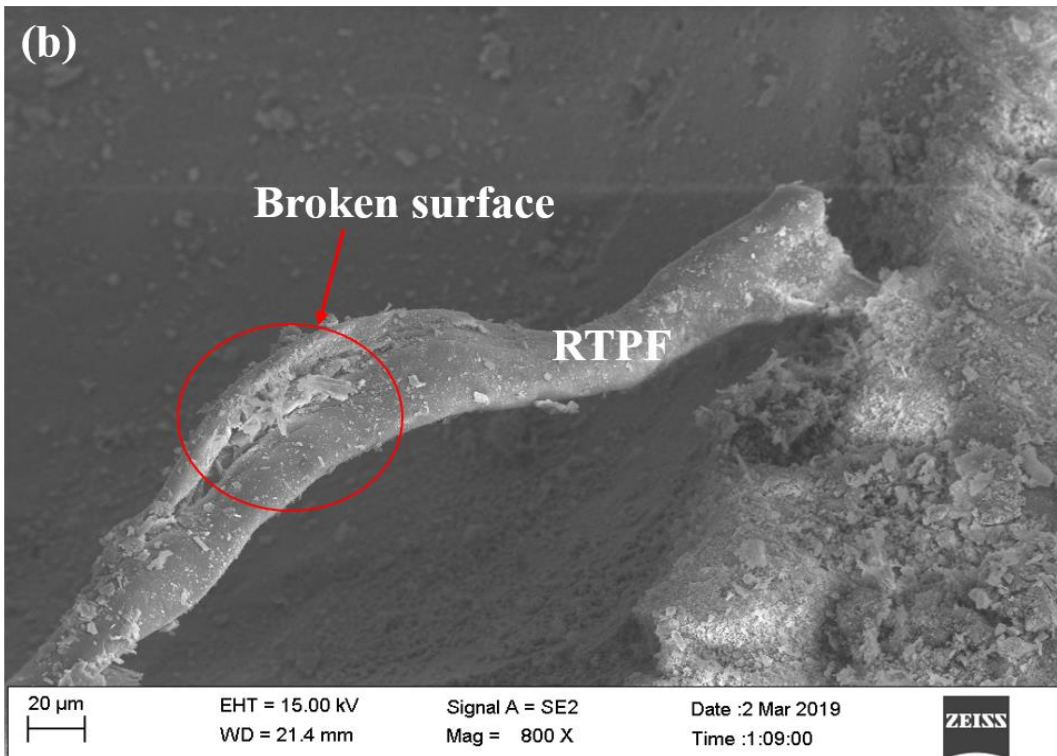
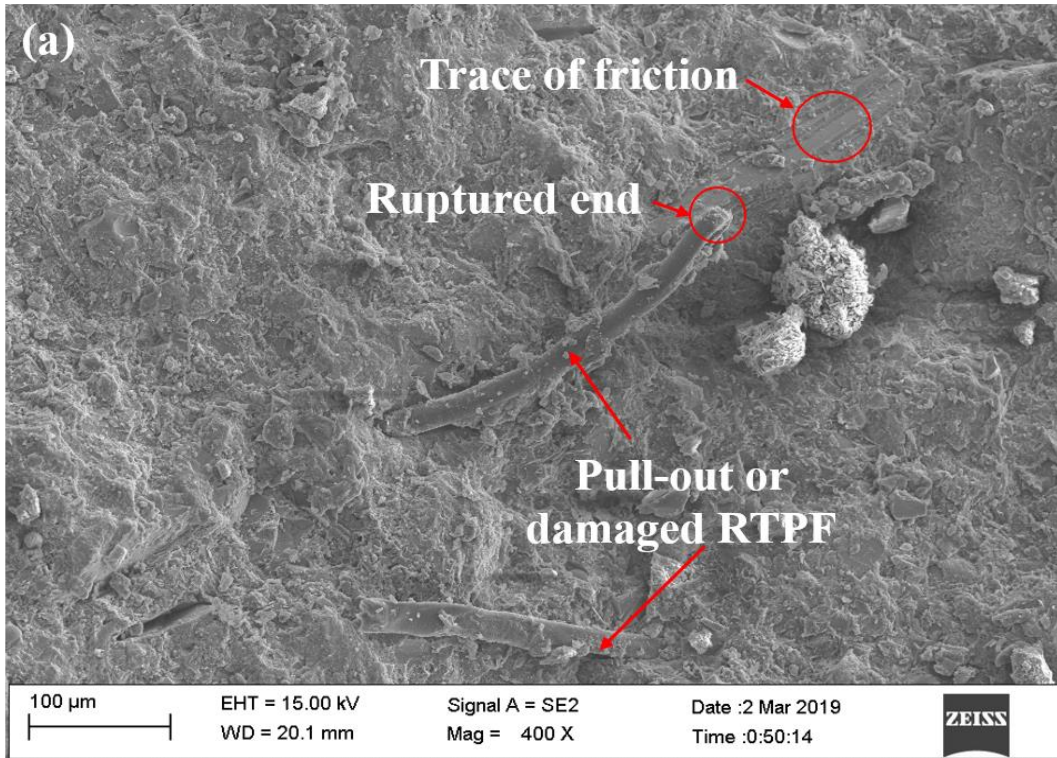


Fig. 17. Cycle ratios of all mixtures at different stages under various stress ratios



**Fig. 18.** Failure modes of all mixtures after flexural fatigue loading ( $S = 0.90$ )



**Fig. 19.** SEM micrographs showing the morphology of RTPF after fatigue failure

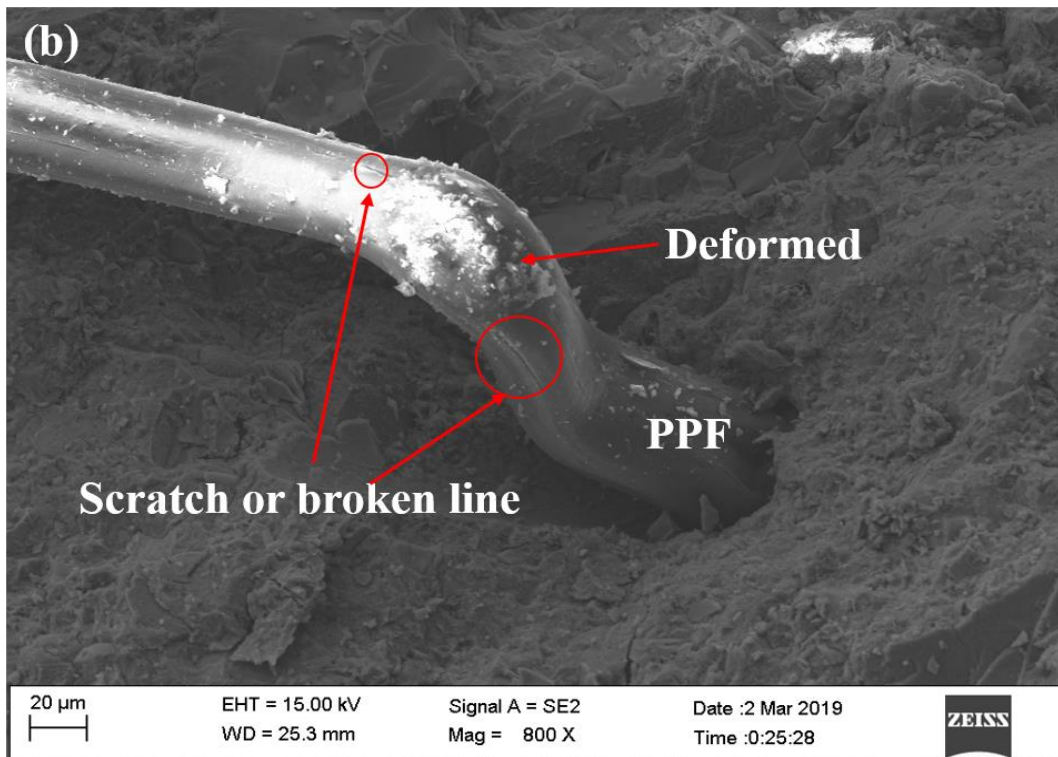
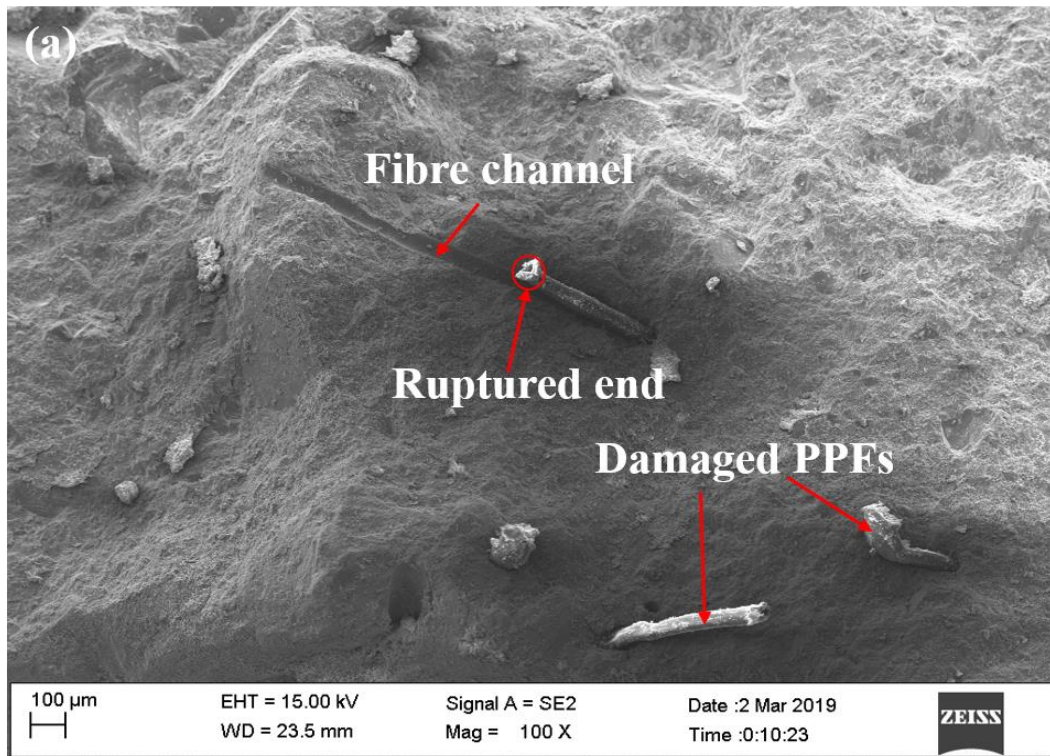


**Fig. 20.** SEM micrographs showing the morphology of PPF after fatigue failure

## Tables

**Table 1.** Chemical compositions (wt%) of cement

Oxide	CaO	SiO <sub>2</sub>	Al <sub>2</sub> O <sub>3</sub>	Fe <sub>2</sub> O <sub>3</sub>	MgO	SO <sub>3</sub>	Na <sub>2</sub> O	LoI
Cement	60.56	21.35	5.98	2.91	2.22	2.05	0.21	4.72

**Table 2.** Properties of fibres used in this study

Fibre type	Length (mm)	Diameter (µm)	Density (kg/m <sup>3</sup> )	Melting point (°C)	Fibre strength (MPa)	Elastic modulus (GPa)
PPF	19	26	910	≥165	376	3.79
RTPF	8.7±4.1	21.1±2.5	1160	≥210	475	3.21

Note: PPF (polypropylene fibre); RTPF (recycled tyre polymer fibre)

**Table 3.** Mixture proportions

Symbol	Cement (kg/m <sup>3</sup> )	FA (kg/m <sup>3</sup> )	CA (kg/m <sup>3</sup> )	Water (kg/m <sup>3</sup> )	SPs (kg/m <sup>3</sup> )	PPF (kg/m <sup>3</sup> )	RTPF (kg/m <sup>3</sup> )
F0	550	560	1128	154	5.5	0	0
PPF09	550	560	1128	154	5.5	0.9 (0.1%)*	0
RTPF12	550	560	1128	154	5.5	0	1.2 (0.1%)*
RTPF24	550	560	1128	154	5.5	0	2.4 (0.2%)*
RTPF48	550	560	1128	154	5.5	0	4.8 (0.4%)*
RTPF96	550	560	1128	154	5.5	0	9.6 (0.8%)*

Note: FA (fine aggregate); CA (coarse aggregate); SPs (superplasticisers); \* (fibre volume fraction, V<sub>f</sub>)

**Table 4.** Testing program for each mixture

No. of sample	Compressive strength test	Flexural strength test	Fatigue test			
			S = 0.90	S = 0.85	S = 0.80	S = 0.75
F0	3	3	5	5	5	5
PPF09	3	3	5	5	5	5
RTPF12	3	3	5	5	5	5
RTPF24	3	3	5	5	5	5
RTPF48	3	3	5	5	5	5
RTPF96	3	3	5	5	5	5

**Table 5.** Summary of Weibull parameters ( $a$  &  $N_a$ ) for all mixtures obtained from different methods

Symbol	Stress level	Graphical method			Method of moments		Maximum likelihood		Average	
		$a$	$N_a$	Correlation coefficient	$a$	$N_a$	$a$	$N_a$	$a$	$N_a$
F0	0.90	0.6613	285	0.9660	1.0305	252	1.0305	252	0.9074	263
	0.85	0.4316	3587	0.9790	0.7260	3369	0.6404	3018	0.5993	3325
	0.80	0.4119	22166	0.9757	0.6967	21597	0.6006	18676	0.5697	20813
	0.75	0.4143	38162	0.9725	0.6927	36962	0.6023	32165	0.5698	35763
RTPF12	0.90	0.6064	354	0.9899	0.9261	314	0.9156	312	0.8160	327
	0.85	0.4033	4780	0.9810	0.7268	4708	0.6027	3982	0.5776	4490
	0.80	0.3682	24079	0.9740	0.6479	24528	0.5379	19789	0.5186	22799
	0.75	0.4040	61420	0.9497	0.8795	53795	0.7059	47556	0.6631	54257
RTPF24	0.90	0.6061	560	0.9893	0.9540	496	0.9351	492	0.8317	516
	0.85	0.4173	12134	0.9849	0.7396	11089	0.6457	9957	0.6009	11060
	0.80	0.4404	60930	0.9376	1.0771	52022	0.8319	46794	0.7831	53249
	0.75	0.4381	176894	0.9895	0.8247	161467	0.7011	145399	0.6546	161253
RTPF48	0.90	0.6437	665	0.9774	0.8968	582	0.9381	595	0.8262	614
	0.85	0.4439	16025	0.9935	0.7897	14133	0.7087	13194	0.6474	14451
	0.80	0.4373	82165	0.9747	0.9287	74328	0.7432	66016	0.7031	74170
	0.75	0.5125	261640	0.9376	0.8467	239368	0.7691	224835	0.7094	241948
RTPF96	0.90	0.7980	179	0.9712	1.2537	159	1.2959	160	1.1159	166
	0.85	0.5036	5609	0.9131	0.7614	5058	0.7248	4839	0.6633	5169
	0.80	0.4928	26818	0.9378	1.0889	22580	0.9205	21164	0.8341	23521
	0.75	0.4104	149522	0.9691	0.8616	140099	0.6748	119733	0.6489	136451
PPF09	0.90	0.7139	425	0.9693	0.9200	368	1.0154	385	0.8831	393
	0.85	0.5125	12011	0.9792	0.6714	8277	0.7293	8859	0.6377	9116
	0.80	0.4602	57004	0.9629	0.8704	25116	0.8065	45444	0.7124	42521
	0.75	0.4691	225661	0.9860	0.8520	209086	0.7326	190291	0.6846	208346

**Table 6.** Developed fatigue equations of all mixtures under different failure probabilities ( $P_f$ )

Symbol	$P_f$	Fatigue equation	Correlation coefficient
F0	0.05	$\lg S = -0.0509 \lg N_p$	0.9554
	0.10	$\lg S = -0.0397 \lg N_p$	0.9228
	0.20	$\lg S = -0.0322 \lg N_p$	0.8851
	0.30	$\lg S = -0.0288 \lg N_p$	0.8637
	0.40	$\lg S = -0.0266 \lg N_p$	0.8488
	0.50	$\lg S = -0.0250 \lg N_p$	0.8370
RTPF12	0.05	$\lg S = -0.0475 \lg N_p$	0.9615
	0.10	$\lg S = -0.0379 \lg N_p$	0.9877
	0.20	$\lg S = -0.0311 \lg N_p$	0.9458
	0.30	$\lg S = -0.0279 \lg N_p$	0.9101
	0.40	$\lg S = -0.0258 \lg N_p$	0.8820
	0.50	$\lg S = -0.0243 \lg N_p$	0.8584
RTPF24	0.05	$\lg S = -0.0357 \lg N_p$	0.9185
	0.10	$\lg S = -0.0306 \lg N_p$	0.9337
	0.20	$\lg S = -0.0265 \lg N_p$	0.9118
	0.30	$\lg S = -0.0244 \lg N_p$	0.8900
	0.40	$\lg S = -0.0230 \lg N_p$	0.8714
	0.50	$\lg S = -0.0219 \lg N_p$	0.8549
RTPF48	0.05	$\lg S = -0.0337 \lg N_p$	0.9778
	0.10	$\lg S = -0.0291 \lg N_p$	0.9619
	0.20	$\lg S = -0.0254 \lg N_p$	0.9256
	0.30	$\lg S = -0.0235 \lg N_p$	0.8993
	0.40	$\lg S = -0.0222 \lg N_p$	0.8786
	0.50	$\lg S = -0.0212 \lg N_p$	0.8611
RTPF96	0.05	$\lg S = -0.0380 \lg N_p$	0.9492
	0.10	$\lg S = -0.0325 \lg N_p$	0.9689
	0.20	$\lg S = -0.0282 \lg N_p$	0.9622
	0.30	$\lg S = -0.0261 \lg N_p$	0.9516
	0.40	$\lg S = -0.0246 \lg N_p$	0.9418
	0.50	$\lg S = -0.0235 \lg N_p$	0.9329
PPF09	0.05	$\lg S = -0.0360 \lg N_p$	0.9864
	0.10	$\lg S = -0.0308 \lg N_p$	0.9843
	0.20	$\lg S = -0.0267 \lg N_p$	0.9567
	0.30	$\lg S = -0.0246 \lg N_p$	0.9344
	0.40	$\lg S = -0.0232 \lg N_p$	0.9164
	0.50	$\lg S = -0.0221 \lg N_p$	0.9010